



The Finite Element
Sea ice-Ocean Model
(FESOM)

Q. Wang et al.

This discussion paper is/has been under review for the journal Geoscientific Model Development (GMD). Please refer to the corresponding final paper in GMD if available.

The Finite Element Sea ice-Ocean Model (FESOM): formulation of an unstructured-mesh ocean general circulation model

Q. Wang, S. Danilov, D. Sidorenko, R. Timmermann, C. Wekerle, X. Wang, T. Jung, and J. Schröter

Alfred Wegener Institute for Polar and Marine Research, Bremerhaven, Germany

Received: 10 June 2013 – Accepted: 27 June 2013 – Published: 23 July 2013

Correspondence to: Q. Wang (qiang.wang@awi.de)

Published by Copernicus Publications on behalf of the European Geosciences Union.

Title Page

Abstract

Introduction

Conclusions

References

Tables

Figures



Back

Close

Full Screen / Esc

Printer-friendly Version

Interactive Discussion



Abstract

The Finite Element Sea ice-Ocean Model (FESOM) is the first global ocean general circulation model based on unstructured-mesh methods that has been developed for the purpose of climate research. The advantage of unstructured-mesh models is their flexible multi-resolution modelling functionality. In this study, an overview of the main features of FESOM will be given; based on sensitivity experiments a number of specific parameter choices will be explained; and directions of future developments will be outlined. It is argued that FESOM is sufficiently mature to explore the benefits of multi-resolution climate modelling and that it provides an excellent platform for further developments required to advance the field of climate modelling on unstructured meshes.

1 Introduction

Climate models are becoming increasingly important to a wider range group of users. They provide projections of anthropogenic climate change; they are extensively used for subseasonal, seasonal and decadal predictions; and they help us to understand the functioning of the climate system.

Despite of substantial progress in climate modelling, even the most sophisticated models still show substantial shortcomings. Simulations of the Atlantic meridional overturning circulation, for example, still vary greatly in strength and pattern between climate models (Randall et al., 2007). Furthermore, many climate models still show substantial problems when it comes to simulating the observed path of the Gulf Stream. It is increasingly being recognized that a lack of sufficiently high spatial resolution is one of the main causes of the existing model shortcomings. In fact, many climate relevant processes are too small-scale in nature to be explicitly resolved by state-of-the-art climate models on available supercomputers and therefore need to be parameterized (Griffies, 2004; Shukla et al., 2009; Jakob, 2010).

The Finite Element Sea ice-Ocean Model (FESOM)

Q. Wang et al.

Title Page

Abstract

Introduction

Conclusions

References

Tables

Figures



Back

Close

Full Screen / Esc

Printer-friendly Version

Interactive Discussion



The Finite Element Sea ice-Ocean Model (FESOM)

Q. Wang et al.

Title Page

Abstract

Introduction

Conclusions

References

Tables

Figures



Back

Close

Full Screen / Esc

Printer-friendly Version

Interactive Discussion



In recent years a new generation of ocean models that employ unstructured-mesh methods has emerged. These models allow to use high spatial resolution in dynamically active regions while keeping a relatively coarse resolution otherwise. It is through this multi-resolution flexibility that unstructured-mesh models provide new opportunities to advance the field of climate modelling. Most existing unstructured-mesh models have dealt with coastal or regional applications (e.g. Chen et al., 2003; Fringer et al., 2006; Zhang and Baptista, 2008).

This paper focuses on the setting of unstructured-mesh models for global applications, that is, on configurations more geared towards climate research related applications. More specifically, the latest version of the Finite Element Sea ice-Ocean Model (FESOM) – the first mature, *global* sea ice-ocean model that employs unstructured-mesh methods – will be described in detail. The fact that FESOM solves the hydrostatic primitive equations for the ocean and comprises a finite element sea ice module makes it an ideal candidate for climate research related applications. FESOM has been developed at the Alfred Wegener Institute, Helmholtz Center for Polar and Marine Research (AWI) over the last 10 yr (Danilov et al., 2004; Wang et al., 2008; Timmermann et al., 2009).

The present study is meant to give a thorough overview of FESOM. Providing the climate modelling community with such an overview of the most mature global multi-resolution sea ice-ocean model seems justified given that unstructured mesh modelling does not feature yet in standard textbooks on ocean modelling. Furthermore, the field is advancing so rapidly that details of the implementation of FESOM described in previous papers (Danilov et al., 2004; Wang et al., 2008; Timmermann et al., 2009) is already slightly outdated. It is also expected that other modelling groups working on the development of similar models (e.g. Ringler et al., 2013) will benefit from a detailed overview of our implementation of unstructured mesh methods in global models. Finally, we expect that the present study, which also entails details on parameterizations and model tuning, will stimulate discussions and therefore ultimately advance the development of multi-resolution models.

The Finite Element Sea ice-Ocean Model (FESOM)

Q. Wang et al.

Title Page

Abstract

Introduction

Conclusions

References

Tables

Figures

⏪

⏩

◀

▶

Back

Close

Full Screen / Esc

Printer-friendly Version

Interactive Discussion



The basic numerical formulation of FESOM including spatial and temporal discretization is described in Sect. 2 together with a brief historical review of FESOM's development. Section 3 represents the key elements of FESOM which are fundamental in formulating ocean climate models. This section partly takes a review form describing various physical parameterizations and numerical methods presented in the literature. A short summary will be given in the last section.

2 Numerical core of FESOM

2.1 Spatial discretization

Here we briefly explain the implementation of the finite element method in FESOM. For the detailed description of the implementation one is referred to Wang et al. (2008). The variational formulation with the FE method involves two basic steps. First, the partial differential equations (primitive equations) are multiplied by a test function and integrated over the model domain. Second, the unknown variables are approximated with a sum over a finite set of basis functions. FESOM uses the combination of continuous, piecewise linear basis functions in two dimensions for surface elevation and in three dimensions for velocity and tracers. For example, sea surface elevation η is discretized using basis functions M_i as

$$\eta \simeq \sum_{i=1}^M \eta_i M_i, \quad (1)$$

where η_i is the discrete value of η at grid node i of the 2-D computational mesh. The test functions are chosen the same as basis functions, leading to the standard Galerkin formulation.

In two dimensions FESOM uses triangular surface meshes. Figure 1 shows the schematic of 2-D basis functions on a triangular mesh. The basis function M_i is equal

GMDD

6, 3893–3976, 2013

**The Finite Element
Sea ice-Ocean Model
(FESOM)**

Q. Wang et al.

[Title Page](#)
[Abstract](#)[Introduction](#)[Conclusions](#)[References](#)[Tables](#)[Figures](#)[⏪](#)[⏩](#)[◀](#)[▶](#)[Back](#)[Close](#)[Full Screen / Esc](#)[Printer-friendly Version](#)[Interactive Discussion](#)

to one at grid node i and goes linearly to zero at its neighbor nodes; it equals zero outside the *stencil* formed by the neighbor nodes. The 3-D mesh is generated by dropping vertical lines starting from the surface 2-D nodes, forming prisms which are then cut to tetrahedral elements (Fig. 2). Except for layers adjacent to sloping ocean bottom each prism is cut to three tetrahedra; above sloping bottom not all three tetrahedra are used in order to employ shaved cells, in analogy to the shaved cells used by Adcroft et al. (1997). Keeping the 3-D grid nodes vertically aligned (i.e. all 3-D nodes have their corresponding 2-D surface nodes above them) is necessitated by the dominance of the hydrostatic balance in the ocean.

For a finite-element discretization the basis functions for velocity and pressure (surface elevation in the hydrostatic case) should meet the so-called LBB condition (Ladyzhenskaya, 1969; Babuska, 1973; Brezzi, 1974), otherwise spurious pressure modes can be excited. These modes are similar to the pressure modes of Arakawa A and B grids (Arakawa, 1966). The basis functions used in FESOM for velocity and pressure do not satisfy the LBB condition, so some measures to stabilize the code against spurious pressure modes are required. Note that pressure modes on unstructured meshes are triggered more easily than in finite-difference models and robust stabilization is always needed.

In the early model version the Galerkin-least squares (GLS) method proposed by Codina and Soto (1997) was used to solve the difficulty related to the LBB condition. In the current model version the GLS method is replaced by a pressure projection method described by Zienkiewicz et al. (1999) to circumvent the LBB condition. With the GLS method the iterative solver needs to solve the surface elevation equation and the vertically integrated momentum equations together (Danilov et al., 2004), whereas with the pressure projection method the solution of surface elevation is separated and no barotropic velocity is introduced (Wang et al., 2008). Therefore using the pressure projection method reduces the computational cost. It also leads to a more consistent code, as in the GLS case the horizontal velocity and vertically integrated horizontal

velocity cannot be in the same functional space in the presence of bottom topography, leading to projection errors.

2.2 Temporal discretization

The *advection* term in the momentum equation is solved with the so-called characteristic-Galerkin method (Zienkiewicz and Taylor, 2000), which is effectively the explicit second-order finite-element Taylor Galerkin method. The method is based on taking temporal discretization using Taylor expansion before applying spatial discretization. Using this method with the linear spatial discretization as mentioned above, the leading-order error of the advection equation is still second order and generates numerical dispersion (Durrant, 1999), thus requiring friction for numerical stability.

The *horizontal viscosity* is solved with the explicit Euler forward method (Sect. 3.9). The *vertical viscosity* is solved with the Euler backward method because the forward time stepping for vertical viscosity is unstable with a typical vertical resolution and time step.¹ To ensure solution efficiency, we solve the implicit vertical mixing operators separately from other parts of the momentum and tracer equations.² The *surface elevation* is solved implicitly to damp fast gravity waves, and needs iterative solvers. The *Coriolis force* term uses the semi-implicit method to well represent inertial oscillations.

¹The stability of an explicit Euler forward time stepping method for vertical viscosity requires $\frac{A_v \Delta t}{\Delta z^2} \leq 1/2$, where A_v is the vertical mixing coefficient. A typical time step of $\Delta t = 40$ min and a surface vertical resolution of $\Delta z = 10$ m require $A_v < 0.02 \text{ m}^2 \text{ s}^{-1}$. Vertical mixing coefficients in the surface boundary layer obtained from the KPP scheme can readily be higher than this value locally.

²To guarantee global conservation the vertical diffusion equations are solved using the finite element method. For continuous basis functions the discretized vertical diffusion equations involve horizontal connections through the mass matrix with the time derivative term, and they cannot be solved efficiently. We chose to lump the matrix of time derivative terms (*lumping* means to sum all entries in a row to the diagonal in the matrix). This leads to a decoupled equation for each water column, which can be very efficiently solved.

The Finite Element Sea ice-Ocean Model (FESOM)

Q. Wang et al.

Title Page

Abstract

Introduction

Conclusions

References

Tables

Figures

⏪

⏩

◀

▶

Back

Close

Full Screen / Esc

Printer-friendly Version

Interactive Discussion



The default *tracer advection* scheme is an explicit flux-corrected-transport (FCT) scheme (Sect. 3.5). The *GM parameterization* is incorporated to the model with the Euler forward method (see Sect. 3.10 for the description of the GM parameterization), while the *vertical diffusivity* uses the Euler backward method for the same reason as
 5 for vertical viscosity.

An external iterative solver is called for solving the surface elevation equation. The final momentum and tracer equations have only matrices of time derivative terms on the left hand side of the equations, which can be relatively efficiently solved.³ Overall the dynamics and thermodynamics in the model are staggered in time with a half time
 10 step. That is, the new velocity is used to advect tracers, and the updated temperature and salinity are then used to calculate density.

2.3 History of FESOM and recent development

The first model version was documented by Danilov et al. (2004). In that version the model used the GLS stabilization which required to introduce the barotropic velocity. It needed to be solved for together with the sea surface elevation (as mentioned in
 15 Sect. 2.1). Advection and friction operators for both momentum and tracers were implicit in time, so iterative solvers were called for all equations and particularly needed to be pre-conditioned in every time step. Overall, the approach proved to be too slow for climate scale simulations.

The issue of model efficiency prompted the model development team to pursue different numerical formulations (Wang et al., 2008). With the purpose to build up a more efficient and robust ocean model, the pressure projection method was adopted to decouple the solution of surface elevation and velocity, the momentum advection and lateral diffusivity and viscosity terms were changed to explicit schemes, the FCT tracer
 20 advection scheme was introduced, the hybrid grid functionality was developed, and

³Implicit advection and lateral friction would require iterative solvers with pre-conditioning in every time step, thus slowing down the solution.

The Finite Element Sea ice-Ocean Model (FESOM)

Q. Wang et al.

Title Page

Abstract

Introduction

Conclusions

References

Tables

Figures



Back

Close

Full Screen / Esc

Printer-friendly Version

Interactive Discussion



some physical parameterizations were incorporated. All these features are kept in the current model version. Further experience was obtained through the work of Timmermann et al. (2009), who concentrated on coupling a finite-element sea-ice model to the ocean code. Since that work was initiated before the work reported in Wang et al. (2008), it was based on a preliminary ocean model code void of most of model updates except for the pressure projection method.

The explored model features from Wang et al. (2008) and Timmermann et al. (2009) have been combined afterwards. For the sake of model development the prism elements (see Fig. 2a) were used in Wang et al. (2008). In prisms basis functions are bilinear (horizontal by vertical) on z -level grids, which allows one to carry out analytical computations of integrals. They deviate from bilinear on general meshes (like sigma grids or shaved prisms) and require to use slower quadrature rules. The code should handle these situations separately for the purpose of high numerical efficiency and proves to be inconvenient to maintain. In contrast, tetrahedral elements always allow for analytical integration. The final model hence uses tetrahedral elements as illustrated in Fig. 2b. The new model version is about 10 times faster than the early version described in Danilov et al. (2004).⁴

There have been a few accomplishments with FESOM development since the last FESOM reports in Wang et al. (2008) and Timmermann et al. (2009). First, a finalized model version combining features obtained during the past development phase is released. It remains stable with respect to its dynamical core over past three years and is recently employed in a coupled climate model. Second, the functionality of modeling ice shelves is added (Sect. 3.13), which utilizes a hybrid grid (Sect. 3.2). Third, the full free surface formulation is added (Sect. 3.12). This is the recommended option for future applications. Finally, in contrast to the earlier development phase when our focus

⁴After taking the new numerical strategies the model is still about 10 times slower than a typical structured-mesh model (Danilov et al., 2008). The run-time memory access, hindered by 1-D storage strategy of FESOM, is one of possible bottlenecks. It still needs some software engineering work to identify the potential in improving model efficiency.

was mostly on the numerical core, more attention is paid to verifying parameterizations and evaluating global models (Sidorenko et al., 2011; Wang et al., 2012; Scholz et al., 2013). Although the development of FESOM has reached a milestone, much research is still required on the route of our model development as to be outlined along the discussions in Sect. 3.

3 Key elements of the model

Different numerical and parameterization schemes are available in FESOM. A detailed description of all the available features of FESOM goes beyond the scope of the present study. Here the focus will be on those model elements that are crucial for climate scale applications.

All sensitivity tests presented in this section are based on atmospheric forcing fields taken from the inter-annual CORE-II data provided by Large and Yeager (2009). All simulations were carried out for 60 yr over the period of forcing provided by Large and Yeager (2009).

3.1 Two-dimensional mesh

FESOM uses spherical coordinates, so the meridional and zonal velocities would be poorly approximated on a triangle covering the North Pole. To avoid the singularity a spherical coordinate system with the north pole over Greenland (40° W, 75° N) is used.⁵

FESOM uses triangular surface meshes. There are a few free triangle-mesh generators available, including DistMesh (Persson and Strang, 2004) and Triangle (Shewchuk, 1996). The mesh quality, the extent to which the triangles are close to equilateral ones, can be further improved after mesh generation by relaxation of grid point locations. An

⁵The three Euler angles for performing the rotation are (50°, 15°, -90°) with the z-x-z rotation convention.

The Finite Element Sea ice-Ocean Model (FESOM)

Q. Wang et al.

Title Page

Abstract

Introduction

Conclusions

References

Tables

Figures



Back

Close

Full Screen / Esc

Printer-friendly Version

Interactive Discussion



abrupt change in resolution can lead to bad triangles (with too small/big inner angles and very different edge lengths) thus degrading the quality of meshes, so a transition zone between high and coarse resolutions is generally introduced. The resolution of an triangle is defined as its minimum height.

5 In practical applications with limited computational resources, we keep the horizontal mesh resolution coarse in most parts of the global ocean (for example, at nominal one degree as used in popular climate models), and refine particularly chosen regions. The equatorial band with meridionally narrow currents and equatorially trapped waves requires higher resolution on the order of $1/3^\circ$ (Latif et al., 1998; Schneider et al., 2003).
10 Figure 3 shows the horizontal resolution of an example mesh with increased resolution in the equatorial band. It is nominal one degree in most parts of the ocean and increases to 24 km poleward of 50° N. The resolution of this mesh is designed in terms of both kilometer (north of 50° N) and geographical degree (south of 50° N) as a particular example, although it is not necessarily so in general cases. Thanks to the flexibility
15 of unstructured meshes, one can fully avoid the imprint of geographic coordinates and design meshes based on distances along the spherical surface.

Many key passages between ocean basins such as Indonesian Throughflow, Bering Strait and Canadian Arctic Archipelago (CAA) are important for basin exchange but narrow and difficult to resolve in global models. Figure 4 shows an example mesh which
20 was configured to study the Arctic Ocean freshwater circulation (Wekerle et al., 2013b). This global mesh uses a coarse resolution south of 50° N and increases resolution to 24 km poleward, with the CAA region resolved at a 5 km scale. Traditional climate models cannot resolve the straits as narrow as in the CAA (27–53 km wide at the narrowest locations in the two largest CAA passages), so they are usually widened
25 and/or deepened to allow adequate throughflow. However, such empirical treatment of CAA results in a very large range in the simulated CAA freshwater transport among a suit of state-of-the-Art ocean models (Jahn et al., 2012). The improved simulation by explicitly resolving the narrow straits with a global FESOM setup indicates the potential

GMDD

6, 3893–3976, 2013

The Finite Element Sea ice-Ocean Model (FESOM)

Q. Wang et al.

Title Page

Abstract

Introduction

Conclusions

References

Tables

Figures



Back

Close

Full Screen / Esc

Printer-friendly Version

Interactive Discussion



of unstructured meshes in representing narrow straits throughflows in global models (Wekerle et al., 2013b).

It is worth mentioning that the model time step size is constrained by the finest resolution on the mesh.⁶ If the number of grid points in the high resolution regions is only a few percent of the total grid points, we cannot enjoy the advantage of using FESOM because the overall time step size has to be set small. Therefore, in practice, increasing horizontal resolution in narrow straits is usually implemented in applications when some part of the ocean basin is also locally refined. In such applications a large portion of the computational grid points are in fine resolution areas. To benefit from the multi-resolution capability even in cases when only a very small portion of the computational grid points have locally increased resolutions, multirate time stepping schemes are needed. Seny et al. (2013) gave an example of such schemes applied in a discontinuous Galerkin model.

3.2 Vertical coordinates and discretization

The choice of vertical coordinates or vertical grids is one of the most important aspects in the design of ocean circulation models (Griffies et al., 2000). Coordinated projects have been carried out to study the performance of different types of vertical discretization, for example, DAMEE-NAB (Chassignet et al., 2000) and DYNAMO (Willebrand et al., 2001). Different vertical coordinates are used in ocean models and each of them has its own advantages and disadvantages (Haidvogel and Beckmann, 1999; Griffies, 2004).

FESOM uses z coordinates (also called geopotential coordinates) in the vertical. The primitive equations are discretized on z *coordinates* without coordinates transformation, while sigma or more general vertical *grids* can be conveniently used because

⁶While an implicit advection scheme is stable in terms of temporal discretization, it is not necessarily accurate if the Courant number ($U\Delta t/\Delta$, where U is the currents speed, Δt is the time step and Δ is the grid spacing) is large.

The Finite Element Sea ice-Ocean Model (FESOM)

Q. Wang et al.

Title Page

Abstract

Introduction

Conclusions

References

Tables

Figures

◀

▶

◀

▶

Back

Close

Full Screen / Esc

Printer-friendly Version

Interactive Discussion



of the FE formulation (Wang et al., 2008). The 2-D mesh and 3-D discretization (including grid types and vertical resolution) are set during the mesh generation stage off-line before carrying out simulations.

Similar to traditional sigma-grid models, truncation errors in computing hydrostatic pressure gradient exist on sigma grids in FESOM (see Sect. 3.4). The error in hydrostatic pressure gradient can be reduced by introducing high order interpolations, but it is not trivial and can potentially degrade the solutions in climate scale simulations. Therefore, z-level grids are recommended in setting up ocean climate models. We use shaved cells over the ocean bottom on z-level grids to better represent the gentle topographic slopes (Adcroft et al., 1997; Wang et al., 2008). A faithful representation of bottom topography by using shaved (or partial) cells can generally improve the integrity of ocean model simulations (Maier-Reimer et al., 1993; Adcroft et al., 1997; Pacanowski and Gnanadesikan, 1998; Myers and Deacu, 2004; Barnier et al., 2006).

Combining z levels in the bulk of the ocean with sigma grids in shelf regions of interest is a viable alternative to z-level grids. A schematic of such hybrid grids is shown in Fig. 5. This type of grids are used in FESOM when the ice cavities are included in the model (Timmermann et al., 2012). This hybrid grid is similar to the generalized coordinate used in POM (Princeton Ocean Model) described by Ezer and Mellor (2004). As illustrated in Fig. 5, sigma grids are used under ice shelf cavities and along the continental shelf around the Antarctic, while the z-levels grids are used in all other parts of the global ocean to minimize pressure gradient errors.

There are a few reasons for using sigma grids in these marginal seas. Sigma grids offer the flexibility in vertical refinement (near the ocean surface, near the bottom, or in the whole column over the shallow continental shelves). The ice-shelf ocean interactions can be better represented with vertically refined resolution near the ocean surface. Increased vertical resolution is also beneficial for representing continental shelf and ocean basins exchange processes, including dense shelf water outflow and circumpolar water inflow. Z-level grids with shaved cells under ice shelves are found to be useful in simulating the ocean circulation in ice cavities (Losch, 2008), while the

GMDD

6, 3893–3976, 2013

The Finite Element Sea ice-Ocean Model (FESOM)

Q. Wang et al.

Title Page

Abstract

Introduction

Conclusions

References

Tables

Figures



Back

Close

Full Screen / Esc

Printer-friendly Version

Interactive Discussion



merits of sigma grids are flexible vertical resolution and less grid scale noise thus less spurious mixing.

On the z -level grid the vertical resolution is usually set finer in the upper 100–200 m depth to better resolve the surface boundary layer and becomes coarser with depth.

Shaved cells are generally used at the bottom. In the region of sigma grids the vertical resolution is set depending on scientific interest, for example, increasing the near surface resolution under the ice shelf and the near bottom resolution where continental shelf and basin water-mass exchange is important. The vertical resolution distribution function of Song and Haidvogel (1994) is used in the mesh generator for adjusting the sigma grid resolution.⁷

3.3 Bottom topography

A blend of several bottom topography datasets is used to provide the bottom topography for FESOM. North of 69° N the 2 km resolution version (version 2) of International Bathymetric Chart of the Arctic Oceans (IBCAO version 2, Jakobsson et al., 2008) is used, while south of 64° N the 1 min resolution version of General Bathymetric Chart of the Oceans (GEBCO) is used. Between 64° N and 69° N the topography is taken as a linear combination of the two datasets. The ocean bottom topography, lower ice surface height and ice shelf grounding line in the ice cavity regions around the Antarctica

⁷A convenient recipe is to define the sigma levels as $z(k) = h_{\min}s(k) + (H - h_{\min})\{(1 - \theta_b)\sinh(\theta s(k))/\sinh(\theta) + \theta_b[\tanh(\theta(s(k) + 0.5)) - \tanh(\theta/2)]/2/\tanh(\theta/2)\}$, where k is the vertical layer index, h_{\min} is the minimum depth in the sigma grid region, H is the water column thickness, $s(k) = -(k - 1)/(N - 1)$ and N is the number of vertical layers (Song and Haidvogel, 1994). $0 \leq \theta \leq 20$ and $0 \leq \theta_b \leq 1$ are the tuning parameters for designing the vertical discretization. Larger θ leads to more refined near surface layers and if θ_b approaches 1 resolution at the bottom is also refined. A transition zone is required to smoothly connect the sigma and z -level grids.

GMDD

6, 3893–3976, 2013

The Finite Element Sea ice-Ocean Model (FESOM)

Q. Wang et al.

Title Page

Abstract

Introduction

Conclusions

References

Tables

Figures

◀

▶

◀

▶

Back

Close

Full Screen / Esc

Printer-friendly Version

Interactive Discussion



are derived from the one minute Refined Topography dataset (Rtopo-1, Timmermann et al., 2010), which is based on the BEDMAP version 1 dataset (Lythe et al., 2001).⁸

The raw topography data are used to determine the ocean coastlines. They are bilinearly interpolated to the model grid points. After the raw topography is interpolated to the model grid, grid scale smoothing of topography is applied to get rid of grid scale noise. The smoothing for each 2-D node is performed over its 2-D stencil (consisting of all 2-D nodes connected by edges with it).⁹ Preliminary smoothing on coarse intermediate meshes should be avoided because it may be too strong for the fine part of the model mesh. One may choose to explicitly resolve narrow ocean straits using locally increased resolution in some cases and apply manual mesh and topography modification at unresolved straits in other cases. Modelers need to decide how to treat individual narrow straits depending on the research interest and overall mesh design.

The topography is bilinearly interpolated from the data grid with fine resolution (2 km and 1 min) to model grids. If the model resolution is much lower than the topography data resolution, adequate smoothing of model topography can have a positive impact on the simulated ocean circulation. It is recommended to repeat the grid scale smoothing several times. Figure 6a and b show the bottom topography after applying stencil smoothing three and one times respectively for the coarse mesh shown in Fig. 3. Sensitivity experiments using these two versions of topography indicate that the former leads to a more realistic ocean circulation (Fig. 7).

⁸Improved ice bed, surface and thickness datasets for Antarctica (BEDMAP2, Fretwel et al., 2013) and a new bathymetry dataset for the Arctic Ocean (IBCAO3, Jakobsson et al., 2012) are released recently and their impact on model simulations compared to previous datasets need to be tested in sensitivity studies.

⁹The smoothing at node i is a weighted mean over its stencil. The neighbor nodes have a weight one and node i has a weight $2n$, where n is the total number of neighbor nodes. As an abrupt change in mesh resolution is avoided, the variation in distance between node i and neighbor nodes is not accounted for in the smoothing.

GMDD

6, 3893–3976, 2013

The Finite Element Sea ice-Ocean Model (FESOM)

Q. Wang et al.

Title Page

Abstract

Introduction

Conclusions

References

Tables

Figures



Back

Close

Full Screen / Esc

Printer-friendly Version

Interactive Discussion



The Finite Element Sea ice-Ocean Model (FESOM)

Q. Wang et al.

Title Page

Abstract

Introduction

Conclusions

References

Tables

Figures

⏪

⏩

◀

▶

Back

Close

Full Screen / Esc

Printer-friendly Version

Interactive Discussion



The barotropic streamfunctions with the two versions of model topography are different mainly in the Southern Ocean, along the western boundary and in the North Atlantic subpolar gyre. In Weddell Sea, the maximum transport in observational estimates is 29.5 Sv along the transect between the northern tip of the Antarctic Peninsula and Kapp Norvegia (Fahrbach et al., 1994) and more than 60 Sv at the Greenwich Meridian (Schroeder and Fahrbach, 1999). Observations suggest mean southward transport at the Labrador Sea exit at 53° N ranging from 37 Sv (Fischer et al., 2004) to 42 Sv (Fischer et al., 2010). Circulations in the Southern Ocean and Labrador Sea are dynamically controlled by the Joint Effect of Baroclinicity and Relief (JEBAR, Olbers et al., 2004; Eden and Willebrand, 2001), so the model results have large sensitivity to the treatment of bottom topography in these places. Because of the relatively coarse mesh (Fig. 3), maximum barotropic transport in these regions is weaker than observed in both simulations. The maximum gyre transport in Weddell Sea and North Atlantic subpolar gyre is about 34 Sv and 28 Sv respectively for the topography shown in Fig. 6a (see Fig. 7a). If topography smoothing is applied only once, the transport is lower by about 10 Sv in both regions (see Fig. 7b).

Over the terrain-following part of the mesh the topography is smoothed by adjusting the slope parameter r_0 (also called Beckmann and Haidvogel number, Beckmann and Haidvogel, 1993) and the hydrostatic inconsistency number r_1 (also called Haney number, Haney, 1991).¹⁰ The smoothing helps to alleviate hydrostatic pressure gradient errors and maintain numerical stability. In practice we recommend the criteria $r_0 \leq 0.2$ and $r_1 \leq 3$. The smoothing is done on each 2-D stencil starting from the shal-

¹⁰ r_0 and r_1 are defined on edges between two neighboring nodes. $r_0 = \frac{|H_i - H_j|}{H_i + H_j}$, where H is the water column thickness, and subscripts i and j indicate two neighboring nodes. $r_1 = \frac{z_i(k) + z_j(k+1) - z_j(k) - z_i(k+1)}{z_i(k) + z_j(k) - z_i(k+1) - z_j(k+1)}$, where $z(k)$ is the vertical coordinate at layer k . The smoothing is done for r_0 first and then for r_1 , over stencils starting from the shallowest depth to the deepest. The smoothing procedure usually needs to be repeated to satisfy the criteria throughout the mesh.

lowest grid point till the deepest grid point. This procedure is repeated until the criteria are satisfied throughout the mesh.

3.4 Hydrostatic pressure gradient

Care should be taken in the calculation of hydrostatic pressure gradient on sigma grids. Pressure gradient errors are not avoidable when the sigma grid surface deviates from the geopotential coordinate, but can be reduced with carefully designed numerics (Shchepetkin and McWilliams, 2003). A few measures are taken to reduce the errors in FESOM. The widely used method of exchanging the sequence of integration and differentiation is employed (Song, 1998; Song and Wright, 1998). The horizontal derivatives of in situ density are taken first and pressure gradient forces are calculated then. In this way pressure gradient force errors are reduced but still present because of truncation errors in representing density with linear functions. The second measure is to use high order interpolation in the vertical to interpolate density to a common depth for computing the density gradient. The idea is discussed and assessed in Wang et al. (2008).

In practice more measures are taken to control the pressure gradient errors on sigma grids. A common additional recipe is to apply topography smoothing to satisfy the criteria for r_0 and r_1 as described in Sect. 3.3. Increasing resolution also helps to reduce pressure gradient errors (Wang et al., 2008). Furthermore, the sigma grid as a part of the hybrid grid is only used around the Antarctic continental shelf and under ice shelves (Section 3.2), where we commonly use increased resolution to resolve small geometrical features.

3.5 Tracer advection

The commonly used tracer advection scheme in FESOM is an explicit second order flux-corrected-transport (FCT) scheme. The classical FCT version described by Löhner et al. (1987) is employed as it works well for transient problems. The FCT scheme

The Finite Element Sea ice-Ocean Model (FESOM)

Q. Wang et al.

Title Page

Abstract

Introduction

Conclusions

References

Tables

Figures



Back

Close

Full Screen / Esc

Printer-friendly Version

Interactive Discussion



preserves monotonicity and eliminates overshoots, a property useful for maintaining numerical stability on eddying scales. Upon comparison to a second order scheme without flux limiter and an implicit second order scheme in idealized two-dimension test cases, at coarse resolution the FCT scheme tends to slightly reduce local maxima even for a smooth field, but it well represents sharp front and shows least dispersion errors in general (Wang, 2007).

Advection schemes should be able to provide adequate dissipation on grid scales and keep large scales less dissipated. Griffies and Hallberg (2000) show that it is important to adequately resolve the admitted scales of motion in order to maintain a small amount of spurious diapycnal mixing in z-coordinate models with commonly used advection schemes. They find that spurious diapycnal mixing can reach more than $10^{-4} \text{ m}^2 \text{ s}^{-1}$ depending on the advection scheme and the flow regime.¹¹ Ilicak et al. (2012) demonstrate that spurious diapycnal transport is directly proportional to the lateral grid Reynolds number. Our preliminary tests show that the effective spurious diapycnal mixing associated with the FESOM FCT scheme is similarly high as shown in Griffies and Hallberg (2000). A systematic research is needed for exploring alternative transport schemes and limiters and for investigating the dependence on the Reynolds number, especially in the context of mesh irregularity.

3.6 Diapycnal mixing

Diapycnal mixing in the ocean has a strong impact on the dynamics of the ocean circulation and on the climate system as a whole (e.g. Bryan, 1987; Park and Bryan, 2000; Wunsch and Ferrari, 2004). The mixing processes are not resolved in present ocean models and need to be parameterized. The *k*-profile parameterization (KPP) proposed by Large et al. (1994) provides a framework accounting for important diapycnal mixing

¹¹The tests by Jochum (2009) indicate that relatively large spurious mixing occurs locally in practice as varying background diffusivity at the order of $0.01 \times 10^{-4} \text{ m}^2 \text{ s}^{-1}$ still produces difference in coarse model results.

The Finite Element Sea ice-Ocean Model (FESOM)

Q. Wang et al.

Title Page

Abstract

Introduction

Conclusions

References

Tables

Figures

⏪

⏩

◀

▶

Back

Close

Full Screen / Esc

Printer-friendly Version

Interactive Discussion



processes, including wind stirring and buoyancy loss at the surface, non-local effects in the surface boundary layer, shear instability, internal wave breaking and double diffusion. Previous studies (Large et al., 1997; Gent et al., 1998) suggest that the KPP scheme is preferable in climate simulations. It is implemented in many current climate models. It is also used in FESOM for large-scale simulations.¹²

Mixing induced by double diffusion (due to salt fingering and double diffusive convection) was found to have a relatively small impact on the mixed layer depth (Danabasoglu et al., 2006) and upper ocean temperature and salinity (Glessmer et al., 2008) in sensitivity studies, although its impact (mainly from salt fingering) on biogeochemical properties is pronounced and cannot be neglected in ecosystem modeling (Glessmer et al., 2008). The double diffusion mixing scheme modified by Danabasoglu et al. (2006) is implemented in FESOM.

3.6.1 Diapycnal mixing from barotropic tides

Mixing due to shear instability is parameterized as a function of Richardson number (Large et al., 1994). To include the mixing from barotropic tides interacting with ocean bottom, especially in the relatively shallow continental shelf regions, the tidal speed is accounted for in the computation of the Richardson number as proposed by Lee et al. (2006). As the tidal speed is large along the coast (Fig. 8), the Richardson number is small and vertical mixing is large in these regions. The original tidal mixing scheme of Lee et al. (2006) leads to too strong vertical mixing even far away vertically from the ocean bottom, as manifested by unrealistic winter polynyas in the central Weddell Sea in our simulations (not shown). The exponential decay as a function of distance from

¹²Other mixing schemes are also used in climate models. For example, the current version of the MPIOM-ECHAM6 Earth System Model (Jungclaus et al., 2013) uses the Pacanowski and Philander (1981) scheme.

The Finite Element Sea ice-Ocean Model (FESOM)

Q. Wang et al.

Title Page

Abstract

Introduction

Conclusions

References

Tables

Figures



Back

Close

Full Screen / Esc

Printer-friendly Version

Interactive Discussion



the ocean bottom suggested by Griffies (2012) is implemented in FESOM. It helps to remove the spurious large mixing.¹³

The barotropic tidal mixing was found to be useful as it assists in the horizontal spreading of river water at certain river mouths (Griffies et al., 2005). Our simulation shows that this is the case especially for the Arctic river runoff. The increased horizontal spreading of river water from the Arctic marginal seas leads to an increase in the freshwater flux at Fram Strait (see Fig. 9). The freshwater transport at Fram Strait shows the largest spread among the four Arctic gates in a recent Arctic Ocean model intercomparison, partly attributed to uncertainties in simulated salinity in the western Arctic Ocean (Jahn et al., 2012). Due to its impact on river water spreading and salinity, tidal mixing is among the key processes that need to be investigated to understand the reported model biases.

Mixing due to barotropic tides has a large-scale impact as it reduces the Atlantic Meridional Overturning Circulation (AMOC) (Fig. 10). The Labrador Sea Water production and AMOC are more sensitive to the freshwater exported through Fram Strait than through Davis Strait (Wekerle et al., 2013b). The increased freshwater export through Fram Strait is an important mechanism through which tidal mixing can consequently weaken the Labrador Sea deep convection and AMOC, while there could be other relevant processes. It should be reminded that the tests shown here are carried out with an ocean-alone model and surface salinity restoring to climatology is enforced. Salinity restoring can provide a local salt sink/source. We speculate that the impact of tidal mixing on the Arctic freshwater export and large scale circulation can differ in coupled climate models (without surface salinity restoring), although the pro-

¹³The parameterization of mixing from barotropic tides interacting with the continental shelf is given by $\kappa_v^{\text{tidal}} = \kappa_{\text{max}}(1 + \sigma Ri)^{-p} \exp^{-(H-|z|)/z_{\text{tide}}}$, where $\kappa_{\text{max}} = 5 \times 10^{-3} \text{ m}^2 \text{ s}^{-1}$, $\sigma = 3$, $p = 1/4$, Ri is the Richardson number based on tidal speed (see Lee et al., 2006, for details), H is the water column thickness, and z_{tide} is an exponential decay length scale (proportional to tidal speed times the M2 tide period). The exponential decay term was introduced by Griffies (2012) and does not exist in the original formula of Lee et al. (2006).

GMDD

6, 3893–3976, 2013

The Finite Element Sea ice-Ocean Model (FESOM)

Q. Wang et al.

Title Page

Abstract

Introduction

Conclusions

References

Tables

Figures

⏪

⏩

◀

▶

Back

Close

Full Screen / Esc

Printer-friendly Version

Interactive Discussion



nounced ocean changes mentioned here imply that climate models should not neglect tide-induced mixing. To include the impact of tides Mueller et al. (2010) added a tidal model into a coupled climate model (MPIOM-ECHAM5). In this case the tidal velocity is simulated and tidal mixing is explicitly taken into account through the dependence of mixing coefficients on the Richardson number. They also reported that tides have pronounced influence on the ocean circulation including weakening of the Labrador Sea deep convection.

3.6.2 Diapycnal mixing associated with internal wave energy dissipation

The background vertical diffusivity in the KPP scheme represents the mixing due to internal wave breaking, which provides mechanical energy to lift cold water across the thermocline and increase the potential energy of water, thus sustaining the large-scale overturning circulation (Huang, 1999; Wunsch and Ferrari, 2004). Wind and tides are the main energy sources for this mechanical energy in the abyss (Munk and Wunsch, 1998). Observational estimates indicate that the diapycnal diffusivity is on the order of $0.12 \pm 0.02 - 0.17 \pm 0.02 \times 10^{-4} \text{ m}^2 \text{ s}^{-1}$ (Ledwell et al., 1993, 1998) in the subtropical Atlantic pycnocline and $0.15 \pm 0.07 \times 10^{-4} \text{ m}^2 \text{ s}^{-1}$ in the North Pacific Ocean (Kelley and Van Scoy, 1999), and much smaller values were observed near the equator (Gregg et al., 2003). In the deep ocean the diffusivity is observed to be small ($0.1 \times 10^{-4} \text{ m}^2 \text{ s}^{-1}$) over smooth topography and much larger ($1 - 5 \times 10^{-4} \text{ m}^2 \text{ s}^{-1}$) near the bottom in regions of rough topography (Polzin et al., 1997; Toole et al., 1997; Ledwell et al., 2000; Morris et al., 2001; Laurent et al., 2012).

A modified version of the Bryan and Lewis (1979) background vertical tracer diffusivity is used poleward of 15° in the model formulation with FESOM (Fig. 11).¹⁴ The minimum value is $0.1 \times 10^{-4} \text{ m}^2 \text{ s}^{-1}$ at the surface and the maximum value is $1.1 \times 10^{-4} \text{ m}^2 \text{ s}^{-1}$ close to the ocean bottom. Motivated by observations (Gregg et al.,

¹⁴The background vertical tracer diffusivity poleward of 15° N/S is computed as a function of depth $\{0.6 + 1.0598/\pi \times \text{atan}[4.5 \times 10^{-3} \times (|z| - 2500.0)]\} \times 10^{-4}$.

The Finite Element Sea ice-Ocean Model (FESOM)

Q. Wang et al.

Title Page

Abstract

Introduction

Conclusions

References

Tables

Figures

◀

▶

◀

▶

Back

Close

Full Screen / Esc

Printer-friendly Version

Interactive Discussion



The Finite Element Sea ice-Ocean Model (FESOM)

Q. Wang et al.

Title Page

Abstract

Introduction

Conclusions

References

Tables

Figures

⏪

⏩

◀

▶

Back

Close

Full Screen / Esc

Printer-friendly Version

Interactive Discussion



2003) the magnitude of this vertical profile is made one order smaller within the $\pm 5^\circ$ latitude range ($0.01 \times 10^{-4} \text{ m}^2 \text{ s}^{-1}$ at ocean surface) and increased linearly to the off-equator value at 15° N/S . Using a coupled climate model Jochum et al. (2008) found that using the small background vertical diffusivity ($0.01 \times 10^{-4} \text{ m}^2 \text{ s}^{-1}$) in the equatorial band improves the tropical precipitation, although the improvement is only minor compared to existing biases. We use a constant background vertical viscosity of $10^{-4} \text{ m}^2 \text{ s}^{-1}$, and there is no observational justification for this value.

Enhanced vertical mixing in the thermocline arising from Parametric Subharmonic Instability (PSI) of the M2 tide at the 28.9° N/S band (Tian et al., 2006; Alford et al., 2007; Hibiya et al., 2007) is not accounted in our model formulation. The model sensitivity study by Jochum et al. (2008) shows that increasing the off-equator background vertical diffusivity in the thermocline toward the observational estimate ($0.17 \times 10^{-4} \text{ m}^2 \text{ s}^{-1}$ instead of $0.1 \times 10^{-4} \text{ m}^2 \text{ s}^{-1}$) or accounting for the mixing arising from PSI worsens the North Atlantic results in their particular tests. Anyway, observations for diapycnal diffusivity have motivated the utilization of more realistic diffusivity values in present climate models (see, e.g. Danabasoglu et al., 2012).

The importance of the Arctic Ocean in the climate system especially in a warming world and the reported difficulty in robustly representing the surface and deep circulation in the Arctic Ocean in state-of-the-Art ocean models (e.g. Karcher et al., 2007; Zhang and Steele, 2007; Jahn et al., 2012) warrant research on improving numerical models including diapycnal mixing parameterizations. The diapycnal mixing in the halocline in the central Arctic Ocean is small compared to mid latitude, largely due to the presence of sea ice (Rainville and Winsor, 2008; Fer, 2009). The diapycnal diffusivity is $0.05 \pm 0.02 \times 10^{-4} \text{ m}^2 \text{ s}^{-1}$ averaged over 70–220 m depth in the Amundsen Basin and as low as $0.01 \times 10^{-4} \text{ m}^2 \text{ s}^{-1}$ in the upper cold halocline (Fer, 2009). A small background vertical diffusivity of $0.01 \times 10^{-4} \text{ m}^2 \text{ s}^{-1}$ was used in the KPP scheme and found to be optimal in some regional Arctic models (Zhang and Steele, 2007; Nguyen et al., 2009). The decrease in diapycnal diffusivity in the Arctic Ocean was taken into account in present climate models (e.g. Jochum et al., 2013). In our practice we found that

The Finite Element Sea ice-Ocean Model (FESOM)

Q. Wang et al.

Title Page

Abstract

Introduction

Conclusions

References

Tables

Figures

◀

▶

◀

▶

Back

Close

Full Screen / Esc

Printer-friendly Version

Interactive Discussion



Energy associated with mesoscale eddies is one more importance source for turbulent mixing. Saenko et al. (2012) have recently investigated the individual effects of the tide and eddy dissipation energies on the ocean circulation. They showed that the overturning circulation and stratification in the deep ocean are too weak when only the tidal energy maintains diapycnal mixing. With the addition of the eddy dissipation, the deep-ocean thermal structure became closer to that observed and the overturning and stratification in the abyss became stronger. Jochum et al. (2013) developed a parameterization for wind-generated near-inertial waves (NIW) and found that tropical sea surface temperature and precipitation and midlatitude westerlies are sensitive to the inclusion of NIW in their climate model. They concluded that because of its importance for global climate the uncertainty in the observed tropical NIW energy needs to be reduced. Presumably the recent progress in the understanding of diapycnal mixing processes will increase model overall fidelity when practical parameterizations for these processes are taken into account.

3.7 Penetrative shortwave radiation

The infrared radiation from the solar heating is almost completely absorbed in the upper 2 m water column, while the ultraviolet and visible part of solar radiation (wavelengths < 750 nm) can penetrate deeper into the ocean depending on the ocean color. In the biologically unproductive waters of the subtropical gyres, solar radiation can directly contribute to the heat content at depths greater than 100 m. Adding all the solar radiation to the uppermost cell in ocean models with a vertical resolution of 10 m or finer can overheat the ocean surface in regions where the penetration depth is deep in reality.

Many sensitivity studies have shown that adequately accounting for shortwave radiation penetration and its spacial and seasonal variation is important for simulating sea surface temperature (SST) and mixed layer depth at low latitude, equatorial undercurrents, and tropical cyclones and El Niño–Southern Oscillation (ENSO) (Schneider and Zhu, 1998; Nakamoto et al., 2001; Rochford et al., 2001; Murtugudde et al., 2002; Timmermann et al., 2002; Sweeney et al., 2005; Marzeion et al., 2005; Anderson et al.,

The Finite Element Sea ice-Ocean Model (FESOM)

Q. Wang et al.

Title Page

Abstract

Introduction

Conclusions

References

Tables

Figures

⏪

⏩

◀

▶

Back

Close

Full Screen / Esc

Printer-friendly Version

Interactive Discussion



2007; Ballabrera-Poy et al., 2007; Zhang et al., 2009; Jochum et al., 2010; Gnanadesikan et al., 2010; Liu et al., 2012). The solar radiation absorption is influenced by ocean color on a global scale, so the bio-physical feedbacks have a global impact on the simulated results, including sea-ice thickness in the Arctic Ocean and the MOC (Lengaigne et al., 2009; Patara et al., 2012).

One traditional way to account for the spacial variation of shortwave penetration in climate models is to use spatially varying attenuation depths in an exponential penetration profile, which was found to be preferable compared to using a constant depth (Murtugudde et al., 2002). The seasonal variability of the attenuation depth plays an important role in the interannual variability in the tropical Pacific (Ballabrera-Poy et al., 2007). The interannual variability in shortwave absorption was also found to be important in representing ENSO in climate models (Jochum et al., 2010).

We use the shortwave penetration treatment as suggested by Sweeney et al. (2005) and Griffies et al. (2005). The optical model of Morel and Antoine (1994) is used to compute visible light absorption.¹⁵ The chlorophyll seasonal climatology of Sweeney et al. (2005) (see Fig. 12) is used in the computation. The visible light attenuation profile is obtained from the optical model, and the difference between two vertical grid levels is used to heat the cells in between. Sweeney et al. (2005) show that the optical models of Morel and Antoine (1994) and Ohlmann (2003) produce relatively small difference in their ocean model.

In some Earth System Models ecosystem models are used to better represent chlorophyll fields and the bio-physical feedbacks (Lengaigne et al., 2009; Loeptien et al., 2009; Jochum et al., 2010; Patara et al., 2012). Prognostic biogeochemistry is potentially beneficial in improving the fidelity of climate prediction through adaptive

¹⁵The attenuation profile of downward radiation in the visible band is computed via $I_{\text{VIS}}(x, y, z) = I_{\text{VIS}}^0(x, y)(V_1 e^{z/\zeta_1} + V_2 e^{z/\zeta_2})$, where V_1 , V_2 , ζ_1 and ζ_2 are computed from an empirical relationship as a function of chlorophyll-a concentration as suggested by Morel and Antoine (1994). I_{VIS}^0 is 54% of the downward solar radiation to the ocean, and the other part is infrared radiation and is directly added to the ocean surface.

bio-physical feedbacks. An ecosystem model (REcoM, Schartau et al., 2007) has just been coupled to FESOM but is not included in the shortwave penetration parameterization in the present model version.

3.8 Vertical overturning

5 The hydrostatic approximation necessitates the use of a parameterization for unresolved vertical overturning processes. One approach is to use the convection adjustment schemes from Cox (1984) or Rahmstorf (1993). The latter scheme can efficiently remove all static instability in a water column. Another approach is to use a large vertical mixing coefficient (e.g. $10 \text{ m}^2 \text{ s}^{-1}$) to quickly mix vertically unstable water columns and it is employed in FESOM.¹⁶ As indicated by Klinger et al. (1996), using a large but
10 finite vertical mixing coefficient can improve the simulation compared to instantaneous convection adjustment. Note that the vertical diffusion approach can only be realized through implicit time stepping.¹⁷

3.9 Horizontal viscosity

15 Horizontal momentum friction in ocean models is employed mainly for practical computational reasons and not motivated by first principles (see the review of Griffies et al., 2000). As a numerical closure, horizontal friction is intended to suppress grid noise associated with the grid Reynolds number and to resolve viscous boundary currents (Bryan et al., 1975; Large et al., 2001; Smith and McWilliams, 2003).¹⁸ In practice,

¹⁶Super-parameterization as an alternative is found to be greatly superior to the convection adjustment parameterization at much less computational cost than running non-hydrostatic models (Campin et al., 2011). Its potential in climate modelling needs to be explored.

¹⁷Implicit time stepping methods for vertical diffusion are needed in general. See footnote 1.

¹⁸In the case of Laplacian viscosity the grid Reynolds number is defined as $Re = U\Delta/A$, where U is the speed of the currents, Δ is the grid resolution, and A is the viscosity. In one dimension, the centered discretization of momentum advection requires $Re < 2$ (or $A > U\Delta/2$) to suppress

The Finite Element Sea ice-Ocean Model (FESOM)

Q. Wang et al.

Title Page

Abstract

Introduction

Conclusions

References

Tables

Figures

◀

▶

◀

▶

Back

Close

Full Screen / Esc

Printer-friendly Version

Interactive Discussion



horizontal friction in climate models is kept as small as feasible provided the grid noise is at an acceptable level and the western boundary layers are properly resolved.

Both Laplacian and biharmonic momentum friction operators are used in large-scale ocean simulations, and there is no first principle motivating either form. With respect to the dissipation scale-selectivity, the biharmonic operator is favorable compared to the Laplacian operator as it induces less dissipation at the resolved scales and concentrates dissipation at the grid scale (Griffies and Hallberg, 2000; Griffies, 2004). Large et al. (2001) and Smith and McWilliams (2003) proposed an anisotropic viscosity scheme by distinguishing the along and cross-flow directions in strong jets in order to reduce horizontal dissipation while satisfying the numerical constraints. Larger zonal viscosities were used in the equatorial band to maintain numerical stability in the presence of strong zonal currents, and larger meridional viscosities were employed along the western boundaries to resolve the Munk boundary layer (Munk, 1950), while the meridional viscosity remained small in the equatorial band to better capture the magnitude and structure of the equatorial current. This approach was adopted in the previous GFDL climate model (Griffies et al., 2005), while isotropic viscosities are restored in a new GFDL Earth System Model to “allow more vigorous tropical instability wave activity at the expense of adding zonal grid noise, particularly in the tropics” (Dunne et al., 2012).

Different choices for viscosity values were made in different ocean climate models. One choice is to use the prescribed viscosity. Due to the convergence of the meridians grid resolution also varies on structured-meshes in some traditional models. To avoid numerical instability associated with large viscosity in an explicit time stepping scheme, viscosity is often scaled with a power of the grid spacing (e.g. Bryan et al., 2007; Hecht et al., 2008). Another approach is to use flow dependent Smagorinsky

the dispersion errors. The second constrain $A > (\sqrt{3}/\pi)^3 \beta \Delta^3$ ensures that the frictional western boundary is resolved by at least one grid point (Bryan et al., 1975). Here β is the meridional gradient of the Coriolis parameter. Additionally, an explicit time stepping (Euler forward) method enforces an upper bound for horizontal viscosity, i.e. $A < \Delta^2 / (2\Delta t)$.

GMDD

6, 3893–3976, 2013

The Finite Element Sea ice-Ocean Model (FESOM)

Q. Wang et al.

Title Page

Abstract

Introduction

Conclusions

References

Tables

Figures

⏪

⏩

◀

▶

Back

Close

Full Screen / Esc

Printer-friendly Version

Interactive Discussion



The Finite Element Sea ice-Ocean Model (FESOM)

Q. Wang et al.

Title Page

Abstract

Introduction

Conclusions

References

Tables

Figures

⏪

⏩

◀

▶

Back

Close

Full Screen / Esc

Printer-friendly Version

Interactive Discussion



viscosities (Smagorinsky, 1963, 1993). The Smagorinsky viscosity is proportional to the local horizontal deformation rate times the squared grid spacing in case of the Laplacian operator. It is enhanced in regions of large horizontal shear, thus providing increased dissipation where it is required to maintain stability. Its dependence on grid spacing eliminates the requirement for additional scaling as done for a priori specified viscosities.

We use the biharmonic friction with a Smagorinsky viscosity in FESOM large scale simulations. Griffies and Hallberg (2000) provide a thorough review on this scheme. As linear (first order) basis functions are used in FESOM, a direct formulation of the biharmonic operator cannot be achieved. Therefore, a two-step approach (first evaluating nodal Laplacian operators, then constructing the biharmonic operators) is used as described by Wang et al. (2008). The biharmonic Smagorinsky viscosity is computed as Laplacian Smagorinsky viscosity times $\Delta^2/8$ as suggested from the linear stability analysis (Griffies and Hallberg, 2000),¹⁹ where Δ is the local grid resolution. The dimensionless scaling parameter in the computation of Smagorinsky viscosity is set equal to π in our practice. To resolve the western boundaries, a minimum biharmonic viscosity of $\beta\Delta^5$ is set at the four grid points close to the western boundaries, where β is the meridional gradient of the Coriolis parameter. When grid resolution is increased along the western boundaries and the velocity becomes more vigorous, the western boundary constrain becomes less stringent than the Reynolds constraints (see the discussion in Griffies and Hallberg, 2000).

Figure 13a shows the sensitivity of barotropic streamfunctions to the two forms of friction operators (biharmonic and Laplacian). The Smagorinsky viscosity is used in both simulations. The difference of barotropic streamfunctions is seen mainly in the Southern Ocean and northern North Atlantic. In both regions the biharmonic viscosity

¹⁹For centered differences in space and forward difference in time in a two dimensions case, the stability requirement is $A < \frac{\Delta^2}{4\Delta t}$ for the Laplacian operator and $B < \frac{\Delta^4}{32\Delta t}$ for the biharmonic operator, thus a ratio of $\Delta^2/8$ between B and A , where A is the Laplacian viscosity, B is the biharmonic viscosity, Δt is the time step, and Δ is the horizontal resolution.

The Finite Element Sea ice-Ocean Model (FESOM)

Q. Wang et al.

Title Page

Abstract

Introduction

Conclusions

References

Tables

Figures

⏪

⏩

◀

▶

Back

Close

Full Screen / Esc

Printer-friendly Version

Interactive Discussion



leads to a stronger circulation, by about 4 Sv for the Antarctic Circumpolar Current (ACC) and 8 Sv for the subpolar gyre in the North Atlantic. Strong and narrow currents are sensitive to the form of friction operators. The strength of North Atlantic Current, South Atlantic Current and Pacific equatorial current is enhanced by 2–4 Sv for the biharmonic case. Local impacts along ACC near topographic features or where the current narrows are also visible.

Consistent with the sensitivity study of Jochum et al. (2008), the boundary currents off east Greenland and west Greenland are enhanced with reduced momentum friction by using the biharmonic operator, thus increasing warm, saline Irminger Current water inflow to the Labrador Sea and decreasing Labrador Sea sea-ice area (not shown).²⁰ Enhanced fraction of Atlantic Water in the Labrador Sea weakens the stratification and results in stronger deep convection there, thus an enhanced AMOC upper cell (by about 1 Sv, see Fig. 14a). The increase in subpolar gyre strength (Fig. 13a) is associated with increased density in the Labrador Sea resulting from enhanced Atlantic Water inflow and deep water ventilation.

More Atlantic Water accumulates south of Greenland-Scotland-Ridge (GSR) in the case of Laplacian friction, leading to stronger deep convection north of 60° N, which is manifested by the strengthening of the overturning circulation at intermediate depth between 50–60° N (Fig. 14a). The commonly called Labrador Sea Water feeding the Deep Western Boundary Current has its origin both in the Labrador Sea and south of GSR including the Irminger Sea (Pickart et al., 2003; Vage et al., 2008; de Jong et al., 2012). Deep mixed layers indicate the presence of deep convection in both regions in both simulations, but reduced dissipation in the biharmonic case favors it in the Labrador Sea. Since reduced dissipation drives both the AMOC and subpolar gyre

²⁰Although a similar conclusion is obtained, our sensitivity tests are different from that of Jochum et al. (2008). They reduce momentum dissipation by replacing the combination of background and Smagorinsky viscosity by only the background one, while we compare the Laplacian friction to the biharmonic friction, with the latter having less dissipation on resolved scales.

strength toward observations in our test, we choose to use the low dissipative biharmonic friction operator. Different regions of the global ocean were analyzed in viscosity sensitivity experiments by Jochum et al. (2008), and generally improved ocean circulations were observed in their coupled climate model with reduced dissipation (at the expense of an increase in numerical noise).

Figures 13b and 14b compare the impact of Smagorinsky and flow-independent, prescribed viscosities. In both simulations the biharmonic friction is used. In the prescribed viscosity case, viscosity is a function of the cubed grid resolution, $B_0\Delta^3/\Delta_0^3$, where $B_0 = -2.7 \times 10^{13} \text{ m}^4 \text{ s}^{-1}$ and $\Delta_0 = 112 \text{ km}$. No obvious instability is visible in both simulations. The difference in the large scale circulation between the two simulations is clearly less significant than for the two friction operators. With the Smagorinsky viscosity the barotropic streamfunction is higher by 2–3 Sv in the central Labrador Sea. The increase in the AMOC upper cell is also rather small (0.1–0.2 Sv). The small difference between the two simulations is not unexpected because the prescribed viscosity is relatively small.

Further evaluation of the impact of momentum dissipation on the large-scale circulation still needs to be pursued, especially for eddy permitting and eddy resolving simulations. For example, an intermediate value of biharmonic viscosity ($0.5B_0\Delta^3/\Delta_0^3$) is found to produce good Gulf Stream separation and realistic North Atlantic Current penetration into the Northwest Corner region in eddy resolving (0.1°) simulations by Bryan et al. (2007). They got a southward displaced Gulf Stream separation with a lower viscosity and large SST errors at the subtropical-subpolar gyre boundary with a higher viscosity, indicating that only a small range in the parameter space exists for tuning their eddy resolving model. To overcome the problems of too early separation of Gulf Stream with a small biharmonic viscosity and establishment of a permanent eddy north of Cape Hatters with a large biharmonic viscosity, Chassignet and Garraffo (2001) and Chassignet and Marshall (2008) recommend to jointly use biharmonic and Laplacian viscosity in eddy resolving models, with both values smaller than those when only one friction form is used. They found that by combining the two operators it is possible to

GMDD

6, 3893–3976, 2013

The Finite Element Sea ice-Ocean Model (FESOM)

Q. Wang et al.

Title Page

Abstract

Introduction

Conclusions

References

Tables

Figures



Back

Close

Full Screen / Esc

Printer-friendly Version

Interactive Discussion



The Finite Element Sea ice-Ocean Model (FESOM)

Q. Wang et al.

Title Page

Abstract

Introduction

Conclusions

References

Tables

Figures

⏪

⏩

◀

▶

Back

Close

Full Screen / Esc

Printer-friendly Version

Interactive Discussion



retain the scale selectiveness of the biharmonic operator and to provide useful damping at larger scales, the latter of which helps to eliminate the wrong permanent eddy. Some recent eddy permitting coupled climate models have chosen to use the biharmonic friction operator (Farneti et al., 2010; Delworth et al., 2012). Providing a unified closure for momentum dissipation valid in various dynamical situations and on meshes refined in different ways and in different regions remains an important and challenging task in developing unstructured-mesh models.

In the sigma grid region in the case of using a hybrid grid, we apply momentum friction along the sigma grid slope to maintain numerical stability.²¹ For unknown reasons the biharmonic operator turns out to be unstable even if it acts along the sigma grid slope. The two-step implementation of the biharmonic operator is presumably the cause for this problem. Therefore we currently employ the Laplacian operator on sigma grids together with the Smagorinsky viscosity.

3.10 Eddy mixing and stirring

Much of the mixing induced by mesoscale eddies is oriented along locally referenced potential density surfaces (neutral surfaces, McDougall, 1987), which has motivated the utilization of rotated tracer diffusion (Redi, 1982; Olbers et al., 1985; Griffies et al., 1998).²² The use of isoneutral diffusion (often called Redi diffusion in literature) significantly reduces the unphysical diapycnal mixing associated with horizontal diffusion (Veronis, 1975; Boning et al., 1995), thus improving model integrity. The neutral dif-

²¹As the sigma grid slope can be very steep, a horizontal friction imposes a large component perpendicular to the grid slope, which can readily lead to instability even with a very small time step in case of a forward time stepping.

²²Neutral diffusion is described by Laplacian operators in ocean climate models, although eddy resolving models use neutral biharmonic operators to add dissipation at grid scales to maintain numerical stability (Roberts and Marshall, 1998). Griffies (2004) provides a thorough review on the properties of biharmonic operators and explains why Laplacian operators are preferable for tracer diffusion.

fusion is the first component of the commonly called GM parameterization (Gent and McWilliams, 1990; Gent et al., 1995, referred to as GM90 hereafter). In the bulk of the ocean interior the neutral slope is small, which motivates the application of the small slope approximation to simplify the diffusion tensor (Gent and McWilliams, 1990).

5 GM90 provided a closure to represent the adiabatic stirring effects of mesoscale eddies, the second component of the GM parameterization. They suggested a form of eddy-induced bolus velocity for z -coordinate models by considering the reduction of available potential energy through baroclinic instability. This bolus velocity is added in tracer equations to advect tracers together with resolved velocity. The implementa-
10 tion of the GM parameterization in z -coordinates models significantly improves the model results including temperature distribution, heat transport and especially deep convection (Danabasoglu et al., 1994; Danabasoglu and McWilliams, 1995; Robitaille and Weaver, 1995; Duffy et al., 1995, 1997; England, 1995; England and Hirst, 1997; Hirst and McDougall, 1996, 1998; Hirst et al., 2000). The eddy-induced velocity as
15 given by GM90 is $\mathbf{v}^* = -\partial_z(\kappa_{\text{gm}}\mathbf{S}) + \hat{\mathbf{z}}\nabla \cdot (\kappa_{\text{gm}}\mathbf{S})$, where κ_{gm} is the GM thickness diffusivity and \mathbf{S} is the neutral slope. It involves computing the derivative of the thickness diffusivity and neutral slope and appears to be noisy in numerical realizations, which is one of the factors that motivated the derivation of the skew flux formulation for eddy-induced transport in Griffies (1998). Using the skew flux formulation also unifies the
20 tracer mixing operators arising from Redi diffusion and GM stirring. It turns out to be very convenient in its implementation in the variational formulation in FESOM. Overall, the small slope approximation for neutral diffusion (Gent and McWilliams, 1990) and the skew diffusion form for eddy stirring (Griffies et al., 1998) are the standard options in the GM parameterization in FESOM.

25 There is a caveat with sigma grids in case of using hybrid grids in FESOM. Because sigma grid slopes and neutral slopes are very different, using GM parameterization will lead to numerical instability on sigma grids. For the moment we use along sigma diffusivity instead of neutral physics. The roles played by mesoscale eddies on continental shelf and in ice cavities around the Antarctic are unclear. In practice we usually use

GMDD

6, 3893–3976, 2013

The Finite Element Sea ice-Ocean Model (FESOM)

Q. Wang et al.

Title Page

Abstract

Introduction

Conclusions

References

Tables

Figures

⏪

⏩

◀

▶

Back

Close

Full Screen / Esc

Printer-friendly Version

Interactive Discussion



high resolution (~ 10 km or finer) for sigma grids, which can eliminate the drawback to some extent.

3.10.1 Diabatic boundary layer

Neutral diffusion represents mesoscale mixing in the adiabatic ocean interior. In the surface diabatic boundary layer where eddies reaching the ocean surface are kinematically constrained to transport horizontally, horizontal diffusion is more physical and should be applied (Treguier et al., 1997). This idea has been commonly taken in ocean climate model practice (e.g. Griffies, 2004; Griffies et al., 2005; Danabasoglu et al., 2008). We use the mixed layer depth (MLD) as an approximation of the surface diabatic boundary layer depth, within which horizontal diffusion is applied. The MLD is defined as the shallowest depth where the interpolated buoyancy gradient matches the maximum buoyancy gradient between the surface and any discrete depth within that water column (Large et al., 1997).

The diffusion tensor is not bounded as the neutral slopes increase, so numerical instability can be incurred when the neutral slopes are very steep. Therefore, the exponential tapering function suggested by Danabasoglu and McWilliams (1995) is applied to the diffusion tensor to change neutral diffusion to horizontal diffusion in regions of steep neutral slopes.²³ The same tapering function is also applied to the GM thickness diffusivity κ_{gm} below the MLD to avoid unbounded eddy velocity \mathbf{v}^* , which is proportional to the gradient of neutral slopes.

Within the surface boundary layer we treat the skew flux as implemented by Griffies et al. (2005). The product ($\kappa_{gm}\mathbf{S}$) is linearly tapered from the value at the base of the

²³The tapering function is only applied to the off-diagonal entries of the diffusion tensor, thus maintaining a horizontal diffusion when these entries are tapered to zero. The function suggested by Danabasoglu and McWilliams (1995) is $f(\mathbf{S}) = 0.5(1 + \tanh(\frac{S_{max} - |\mathbf{S}|}{S_d}))$, where $S_d = 0.001$ is the width scale of the tapering function and $S_{max} = 0.05$ is the cut-off value beyond which f decreases to zero rapidly.

The Finite Element Sea ice-Ocean Model (FESOM)

Q. Wang et al.

Title Page

Abstract

Introduction

Conclusions

References

Tables

Figures



Back

Close

Full Screen / Esc

Printer-friendly Version

Interactive Discussion



finite bolus velocity without incurring numerical instability in the surface boundary layer. Sensitivity tests show that using a critical slope larger than 0.1 can entail numerical instability sometimes. Another consideration for the choice of S_{\max} is associated with the tapering function for the ocean interior (see footnote 23). The magnitude of neutral slopes is mostly less than 0.01 below the surface layer, so we have empirically chosen $S_{\max} = 0.05$. As suggested by Gerdes et al. (1991) and Griffies et al. (2005) the GM parameterization is changed back to horizontal diffusion at grid points adjacent to ocean bottom to avoid overshoots in tracer fields.

3.10.2 Neutral and thickness diffusivity

Methods to specify neutral diffusivity and thickness diffusivity differ among ocean climate models, including using a constant value (Danabasoglu et al., 2006), horizontally varying diffusivity depending on vertically averaged flow fields (Visbeck et al., 1997; Griffies et al., 2005), and diffusivity varying in three dimensions depending on flow fields (Danabasoglu and Marshall, 2007; Eden et al., 2009). Estimates from observations (e.g. Ledwell et al., 1998; Bauer et al., 1998; Sundermeyer and Price, 1998; Zhurbas and Oh, 2003; Marshall et al., 2006) and high resolution ocean models (e.g. Bryan et al., 1999; Eden, 2006; Eden et al., 2007) have revealed pronounced variability of eddy diffusivity in space and time. Many numerical and theoretical studies have focused on the prescription for the vertical variation (Danabasoglu and McWilliams, 1995; Killworth, 1997; Treguier, 1999) and horizontal variation (Held and Larichev, 1996; Visbeck et al., 1997; Griffies et al., 2005) of eddy diffusivity. More recent efforts in prescribing eddy diffusivity have focused on schemes of eddy diffusivity varying in three dimensions and time. Motivated by the finding that the squared buoyancy frequency (N^2) shows a vertical structure similar to the diagnosed diffusivity (Ferreira et al., 2005; Eden, 2006; Eden et al., 2007; Ferreira and Marshall, 2006) and Danabasoglu and Marshall (2007) have investigated the impacts of using diffusivity proportional to N^2 in model simulations. Eden and Greatbatch (2008) proposed a closure for eddy thickness

diffusivity consisting of a prognostic equation for the eddy kinetic energy and an eddy length scale.

The N^2 dependent thickness diffusivity as suggested by Ferreira et al. (2005) and Ferreira and Marshall (2006) was implemented in the NCAR Community Climate System Model (CCSM3), and it leads to improved results with respect to observations compared to using a constant diffusivity (Danabasoglu and Marshall, 2007). It is further used in the updated NCAR climate model CCSM4 (Danabasoglu et al., 2012). Currently this approach is also used in FESOM simulations. The thickness diffusivity is calculated as $\kappa_{\text{gm}}(x, y, z, t) = \kappa_{\text{ref}}(x, y)N(x, y, z, t)^2/N_{\text{ref}}(x, y, t)^2$, where $\kappa_{\text{ref}}(x, y)$ is a reference diffusivity at horizontal location (x, y) and $N(x, y, z, t)$ is the local buoyancy frequency. $N_{\text{ref}}(x, y, t)$ is the reference buoyancy frequency taken just below MLD, provided that $N^2 > 0$ there. Otherwise N_{ref}^2 is the first stable N^2 below MLD. Following Danabasoglu and Marshall (2007) the ratio N^2/N_{ref}^2 is constrained by $N_{\text{min}} \leq N^2/N_{\text{ref}}^2 \leq 1$, where N_{min} sets the lower bound for diffusivity. The neutral diffusivity is set equal to the thickness diffusivity below the MLD. Within the MLD the linear tapering is applied to eddy skew flux and the horizontal diffusivity is set to the reference diffusivity.

The reference diffusivity $\kappa_{\text{ref}}(x, y)$ is set to a constant ($1500 \text{ m}^2 \text{ s}^{-1}$) for regions where horizontal resolution is coarser than 50 km, and scaled down when resolution is finer.²⁴ We prescribed the scaling function for diffusivity based on experience obtained so far. Sensitivity tests with 25 km resolution in the Arctic Ocean (where the first baroclinic Rossby radius is less than 8 km in the Eurasian Basin as derived from climatology data, Qun Li, personal communication, 2012) show that using a neutral diffusivity larger than $50 \text{ m}^2 \text{ s}^{-1}$ leads to a too diffused boundary currents in the Arctic Atlantic Water layer.²⁵ Therefore we reduce the reference diffusivity rapidly from $1500 \text{ m}^2 \text{ s}^{-1}$ at 50 km resolution to $50 \text{ m}^2 \text{ s}^{-1}$ at 25 km resolution. The ratio of the first Rossby radius to the

²⁴The reference diffusivity [$\text{m}^2 \text{ s}^{-1}$] is set to 1500 for $\Delta \geq 50$, $50 + 58(\Delta - 25)$ for $25 \leq \Delta < 50$, and $50(\Delta/25)^2$ for $\Delta < 25$. Here Δ is local horizontal resolution with unit km.

²⁵Other parameterizations such as the anisotropic GM parameterization suggested by Smith and Gent (2004) and the Neptune parameterization (Maltrud and Holloway, 2008; Holloway

The Finite Element
Sea ice-Ocean Model
(FESOM)

Q. Wang et al.

Title Page

Abstract

Introduction

Conclusions

References

Tables

Figures

◀

▶

◀

▶

Back

Close

Full Screen / Esc

Printer-friendly Version

Interactive Discussion



grid scale (λ_1/Δ) is a pertinent control parameter for scaling eddy diffusivity. Using it to construct a unified scaling function also needs case-based tuning and remains a research topic.²⁶

We set $N_{\min} = 0.2$, meaning that the diffusivity is confined above $300 \text{ m}^2 \text{ s}^{-1}$ in regions with resolution coarser than 50 km. The time mean thickness diffusivity at 300 m depth on the reference mesh (Fig. 3) is shown in Fig. 15. Largest values are found in regions where intense eddy activity is expected, including the ACC and western boundary currents. Due to the resolution dependence of the reference diffusivity, reduced values are found in the equatorial band and north of 50° N where the grid spacing is small (Fig. 3). As also noticed in Danabasoglu and Marshall (2007), the diffusivity scheme produces undesirable large values in the eastern South Pacific. The zonal-mean distribution (Fig. 16) shows that the diffusivity decreases from the base of surface diabatic layer downwards as expected from vertical distribution of squared buoyancy frequency. Largest values are found in the tropics just below the diabatic layer, with the value in the equatorial band scaled down due to higher horizontal resolution. Deep penetration of large diffusivity occurs at mid to high latitude on both hemispheres, while the deepest penetration is in the Southern Ocean. The deep reaching high diffusivity north of 60° N in Danabasoglu and Marshall (2007) (their Fig. 1, associated with deep convection regions in the North Atlantic) is absent in Fig. 16 because the reference diffusivity is scaled to about $50 \text{ m}^2 \text{ s}^{-1}$ on our reference mesh.

and Wang, 2009) could improve the solution of the Arctic boundary currents. These options also need to be explored in the future.

²⁶In an eddy regime, eddies can transfer tracer variance to the grid scale, and this variance must be dissipated without inducing spurious diapycnal mixing, with the neutral diffusion operator being a possible numerical dissipation form (Roberts and Marshall, 1998; Griffies and Hallberg, 2000; Griffies, 2004). In practice the choice of diffusivity depends on the advection scheme used in the model. By using an improved advection scheme the GM parameterization was completely turned off in ocean-eddy-permitting climate simulations in Farneti et al. (2010) and Farneti and Gent (2011).

The Finite Element
Sea ice-Ocean Model
(FESOM)

Q. Wang et al.

Title Page

Abstract

Introduction

Conclusions

References

Tables

Figures



Back

Close

Full Screen / Esc

Printer-friendly Version

Interactive Discussion



GMDD

6, 3893–3976, 2013

The Finite Element
Sea ice-Ocean Model
(FESOM)

Q. Wang et al.

Title Page

Abstract

Introduction

Conclusions

References

Tables

Figures



Back

Close

Full Screen / Esc

Printer-friendly Version

Interactive Discussion



N_{\min} turns out to be one of the key tuning parameters in the calculation of diffusivity. The residual meridional overturning streamfunctions (Eulerian mean plus eddy contribution parameterized by thickness diffusivity) in the Southern Ocean from simulations with $N_{\min} = 0.2$ and 0.1 are shown in Fig. 17a and b, respectively. Both the Deacon cell and Antarctic Bottom Water (AABW) cell show very similar structures between the two simulations. State estimate using an adjoint eddy-permitting ($1/6^\circ$) model by Mazloff et al. (2010) shows a Southern Ocean Ekman transport of about 31 Sv, a Deacon cell in depth space (Doos and Webb, 1994) reaching more than 3000 m depth and a maximum AABW transport of about 16 Sv (their Fig. 10a). Both simulations reasonably reproduce the meridional overturning circulation structure reported by Mazloff et al. (2010), with some underestimation of the circulation strength of both bottom water and intermediate water. Figure 17c and d compare the parameterized eddy meridional overturning streamfunctions between the two simulations. With a decrease of N_{\min} from 0.2 to 0.1, the eddy MOC maximum reduces from about 10 Sv to 5 Sv. Although decreasing N_{\min} (the lower bound of diffusivity) can have impact on the diffusivity mainly below 1500 m depth for the Southern Ocean region (see Fig. 16), the weakening of the eddy meridional overturning is over the whole water column. Along with the weakening of the eddy-induced transport, the AABW transport also weakens (Fig. 17a and b), consistent with other model results (Farneti and Gent, 2011).

Mesoscale eddies in the Southern Ocean can buffer the ocean response to atmospheric changes (Meredith and Hogg, 2006; Hallberg and Gnanadesikan, 2006; Böning et al., 2008; Farneti et al., 2010; Viebahn and Eden, 2010; Jones et al., 2011; Abernathey et al., 2011; Meredith et al., 2012; Morrison and Hogg, 2013; Munday et al., 2013), so assessing and improving their parameterization in climate models is critically important. It is possible to use the present GM parameterizations to produce a response of the Southern Ocean to changing wind stress in coarse climate models that is broadly consistent with what is seen in eddying ocean models (e.g. Gent and Danabasoglu, 2011). However, eddy parameterizations have only demonstrated some success

The Finite Element Sea ice-Ocean Model (FESOM)

Q. Wang et al.

Title Page

Abstract

Introduction

Conclusions

References

Tables

Figures



Back

Close

Full Screen / Esc

Printer-friendly Version

Interactive Discussion



in reproducing the eddy compensation but not the eddy saturation.²⁷ As remarked by Munday et al. (2013), eddy compensation is achieved at the expense of being not able to realize the eddy saturated regime using the parameterization. Hence they suggested that parameterizations with a prognostic eddy kinetic energy (EKE) variable (Eden and Greatbatch, 2008; Marshall and Adcroft, 2010), which can be tied directly to wind stress, be preferable schemes for thickness diffusivity. However, schemes such as the one proposed by Eden and Greatbatch (2008), while probably a better way to go, assume that the time evolution of EKE can be parameterized in a model. This is not a trivial task as the relationship of changes in EKE to changes in forcing is one of the big unsolved problems.

Attention has been paid to the practical implementation of traditional GM parameterizations. For example, Gnanadesikan et al. (2007) and Farneti and Gent (2011) found that model results are very sensitive to the critical neutral slope in their simulations; some simulated features can be improved at the expense of worsening some other features when increasing the critical neutral slope. These findings also indicate that much research is still required for mesoscale-eddy parameterizations. Ferrari et al. (2010) propose a parameterization for mesoscale eddy transport which solves a boundary value problem for each vertical ocean column. They shows that this scheme works robustly and performs as well as their implementation of the more conventional GM scheme. Further study is required to explore its potential in increasing the fidelity of ocean model simulations.

²⁷*Eddy saturation* refers to the phenomenon that ACC transport shows limited response to increased wind stress. It can be explained by a rough balance between the tendency for Ekman transport to steepen isopycnals and for eddies to flatten them. *Eddy compensation* refers to the phenomenon that changes in eddy-induced meridional overturning circulation can partially compensate those of Ekman transport. These two phenomena are linked but with dynamical distinction (e.g. Morrison and Hogg, 2013).

3.11 River runoff distribution

River discharge is one of the important processes that redistribute water masses in the Earth system. For example, the Arctic Ocean is the largest freshwater reservoir in the global ocean, with 38% of its freshwater source provided by river runoff (Serreze et al., 2006). Faithfully representing the circulation of freshwater supplied by rivers in ocean models is important, but depends on the numerical treatment of the runoff. As reported in Griffies et al. (2005), adding river runoff into the surface grid cell can lead to too much freshwater on the surface stabilizing the water column. It motivated them to insert river runoff into the upper four model grid cells. This approach is a parameterization for unresolved processes that can influence river runoff distribution in reality, including tidal mixing. Due to the current model numerics we did not implement this approach in FESOM. The diapycnal mixing parameterization for barotropic tides proposed by Lee et al. (2006) is a remedy we use to improve river runoff representation, as mentioned in Sect. 3.6.1.

Another approach used in climate models is to spread river runoff over a wide region near river mouths (Danabasoglu et al., 2006). This approach is expected to remedy possibly under-resolved spreading of river runoff at coarse resolution, for example, by eddies. Using a high resolution model McGeehan and Maslowski (2011) showed how eddies transport water-masses of the Labrador Sea boundary current into the gyre interior. The first baroclinic Rossby radius of deformation λ_1 is typically small in coastal regions. For example, λ_1 is on the order of 3 km on the western Arctic shelf, so resolving mesoscale eddies cannot be afforded even in regional models. Arguably adding river runoff over a wide region can be a poor man's approach to account for the under-resolved processes that facilitate freshwater penetration to ocean basins.

Typically we distribute river runoff around river mouths using a linear function decreasing from one at the river mouths to zero at 400 km distance. Figure 18a shows the river runoff distribution of the long-term climatology derived from Dai et al. (2009). We carry out sensitivity tests using this distribution (reference run) and another one

GMDD

6, 3893–3976, 2013

The Finite Element Sea ice-Ocean Model (FESOM)

Q. Wang et al.

Title Page

Abstract

Introduction

Conclusions

References

Tables

Figures

◀

▶

◀

▶

Back

Close

Full Screen / Esc

Printer-friendly Version

Interactive Discussion



The Finite Element Sea ice-Ocean Model (FESOM)

Q. Wang et al.

[Title Page](#)[Abstract](#)[Introduction](#)[Conclusions](#)[References](#)[Tables](#)[Figures](#)[Back](#)[Close](#)[Full Screen / Esc](#)[Printer-friendly Version](#)[Interactive Discussion](#)

where the river runoff is distributed within 100 km distance from river mouths (sensitivity run, Fig. 18b). The difference between the two experiments for salinity at surface and 100 m depth is shown in Fig. 19a and b. As expected, the largest difference is close to river mouths where the difference is directly enforced, with lower salinity immediately at river mouths and higher salinity around them in the sensitivity run.

The impact of applying different river runoff distribution on the Arctic basin develops with time. The salinity in the halocline is characterized by local difference patches of ± 0.1 psu in the Arctic basin (Fig. 19b). The changes of salinity between the two runs are nonuniform with both positive and negative signs, implying that associated changes in local circulation are also responsible for the observed difference in salinity. To assess the significance of the impact from adjusting the river runoff distribution, we compared the difference in salinity in the halocline to that induced by adjusting background vertical diffusivity (changing from the currently used value $0.1 \times 10^{-4} \text{ m}^2 \text{ s}^{-1}$ to $0.01 \times 10^{-4} \text{ m}^2 \text{ s}^{-1}$ as used by Nguyen et al., 2009 and Zhang and Steele, 2007, see discussion in Sect. 3.6.2). We found that the difference obtained here is a few times smaller. Further analysis shows that the freshwater export flux remains almost intact for both Fram Strait and CAA in the sensitivity run, so the impact of applying different river runoff distribution in the Arctic Ocean is mainly limited to the Arctic basin.

Both the temperature and salinity in the North Atlantic subpolar gyre are increased in the sensitivity run (Fig. 19). This is consistent with the strengthening of the AMOC upper cell (Fig. 20), which increases the supply of warm, saline Atlantic Water to the subpolar gyre. As the freshwater export from the Arctic Ocean remains the same, the changes in AMOC are linked to modified river runoff distribution along the North American and Greenland coasts. This is not an unexpected impact as confining river runoff more to the coast will facilitate deep convection in the Labrador Sea thus a stronger AMOC. Although the impact of a wide spreading of river runoff is moderate as tested here, we keep this option in the model.

3.12 Free surface formulation

While rigid-lid ocean models are becoming obsolete, ocean models with the free-surface method and fixed volume for tracer budget have been widely used during the last decade. In the latter type of models, the sea surface height equation has a free surface algorithm whereas tracers cannot experience dilution or concentration associated with ocean volume changes. To have the impact of surface freshwater flux (evaporation, precipitation, river runoff, and freshwater associated with ice/snow thermodynamics) on salinity, a virtual salt flux has to be introduced for the salinity equation as a surface boundary condition. In reality there are no salt changes in the ocean except for changes through storage of salt in sea ice. Therefore the virtual salt flux formulation is unphysical, although it parameterizes most of the effect of surface freshwater flux on surface salinity.

The virtual salt flux is given by $F^{\text{virtual, salt}} = s_{\text{ref}}q_w$, where q_w is total surface freshwater flux and s_{ref} is a reference salinity. If s_{ref} is set to a constant, the ocean salt is conserved upon that the global integral of q_w is zero. A problem with this choice is that the local sea surface salinity can be very different from the reference salinity and the dilution effect of surface freshwater on salinity cannot be well represented in the model. When the local sea surface salinity is far from the reference salinity, virtual salt flux formulation can lead to too small or too large salinity and thus model blowup. Another choice for calculating the virtual salt flux is to use local sea surface salinity as the reference salinity. In this case the local feedback on salinity from freshwater flux is properly simulated, but the total salt conservation in the ocean is not automatically ensured even when the global integral of q_w is zero. One practical remedy for this is to calculate the global integral of virtual salt flux and remove it by subtracting its global mean over the globe during the model runtime. Effectively this remedy alters local salinity unphysically and might spoil model integrity on climate scales.

In a full free surface formulation the ocean volume changes with the vertical movement of surface grid points and tracer concentration directly reacts on these changes.

GMDD

6, 3893–3976, 2013

The Finite Element Sea ice-Ocean Model (FESOM)

Q. Wang et al.

Title Page

Abstract

Introduction

Conclusions

References

Tables

Figures

⏪

⏩

◀

▶

Back

Close

Full Screen / Esc

Printer-friendly Version

Interactive Discussion



improved quality compiled by Timmermann et al. (2010) are used (Sect. 3.3). As shown by Timmermann et al. (2012) and Timmermann and Hellmer (2013), basal mass fluxes are in most cases realistic from the model, but differences from observations suggest that further improvement is still desirable. The major issues are linked to the utilization of sigma grids, including possible distortion to flow dynamics caused by smoothing of bottom bathymetry and ice shelf draft required for reducing pressure gradient errors, requirement for individual numerical formulation of GM parameterization (Sect. 3.10), and missing support for the full free surface option in the sigma grid region (Sect. 3.12). These aspects remain to be explored and improved.

4 Conclusions

Unstructured-mesh models open new horizons for climate modeling: local dynamics can be better resolved with locally increased resolution without traditional nesting and the improved local processes can provide feedback to the large scale circulation. In this paper we give an overview about the formulation of FESOM, which is the first ocean general circulation model that uses unstructured meshes and therefore allows to carry out multi-resolution simulations. We described the key model elements including the two-dimensional mesh, vertical discretization, bottom topography, pressure gradient calculation, tracer advection scheme, diapycnal mixing parameterization, penetrative shortwave treatment, convection adjustment, horizontal momentum friction, GM parameterization, river runoff distribution, free surface formulation and ice shelf modeling. The progress reported here is a result of our own continuing model development efforts as well as the recent advances by the ocean modeling community in general. The model version described here is the standard version for our ocean stand-alone studies and employed as the sea ice-ocean component of a new coupled climate model (Sidorenko et al., 2013).

Along with the model description we briefly reviewed some of the key elements related to ocean climate models. Discussions on the knowledge gained in the community

GMDD

6, 3893–3976, 2013

The Finite Element Sea ice-Ocean Model (FESOM)

Q. Wang et al.

Title Page

Abstract

Introduction

Conclusions

References

Tables

Figures



Back

Close

Full Screen / Esc

Printer-friendly Version

Interactive Discussion



GMDD

6, 3893–3976, 2013

The Finite Element
Sea ice-Ocean Model
(FESOM)

Q. Wang et al.

Title Page

Abstract

Introduction

Conclusions

References

Tables

Figures



Back

Close

Full Screen / Esc

Printer-friendly Version

Interactive Discussion



provide the guideline for making choices in constructing our model. Griffies (2004) has provided a thorough review on ocean model fundamentals. Due to limitations in resources we did not implement or test all numerical and parameterization options recommended in other studies. Investigations to further improve numerical and physical schemes are required as outlined in Sect. 3. There are other model components that should be updated in FESOM, for example, the overflow parameterization (there are different schemes suggested in previous studies, e.g. Beckmann and Döscher, 1997; Danabasoglu et al., 2010). Parameterizations with scale-selectivity are critically important in unstructured-mesh models. We are only beginning to explore the multi-resolution aspects of parameterizations. More sensitivity studies and multi-resolution tests are desirable to improve the formulation and implementation of such parameterizations. We note that broad collaborations, like the on-going international joint project COREs (Griffies et al., 2009; Danabasoglu et al., 2013), are helpful to identify common issues in present state-of-the-art ocean models and consolidate efforts in ocean model development.

In summary, we would argue that unstructured-mesh sea ice-ocean models have matured substantially in recent years. Consequently, they have become attractive options for simulating multi-resolution aspects of the climate system. First climate-relevant applications are appearing (e.g. Wang et al., 2012; Wekerle et al., 2013b,a; Hellmer et al., 2012; Timmermann et al., 2012; Timmermann and Hellmer, 2013). However, further research is urgently required to explore the full potential of multi-resolution modelling in climate research.

Acknowledgement. During our model development we got valuable support from colleagues in the AWI computer center, including Sven Harig, Lars Nerger, Wolfgang Hiller, Stephan Frickenhaus and many others. Many model users provided useful feedbacks which helped improve the code. We thank Richard Greatbatch for helpful comments on the manuscript. Part of the work was financially supported by Helmholtz Climate Initiative REKLIM (Regional Climate Change). The computational resources for this work were provided through the North-German Supercomputing Alliance (HLRN).

References

- Abernathey, R., Marshall, J., and Ferreira, D.: The dependence of Southern Ocean meridional overturning on wind stress, *J. Phys. Oceanogr.*, 41, 2261–2278, 2011. 3929
- Adcroft, A., Hill, C., and Marshall, J.: Representation of topography by shaved cells in a height coordinate ocean model, *Mon. Weather Rev.*, 125, 2293–2315, 1997. 3897, 3904
- Alford, M. H., MacKinnon, J. A., Zhao, Z., Pinkel, R., Klymak, J., and Peacock, T.: Internal waves across the Pacific, *Geophys. Res. Lett.*, 34, L24601, doi:10.1029/2007GL031566, 2007. 3913
- Anderson, W. G., Gnanadesikan, A., Hallberg, R., Dunne, J., and Samuels, B. L.: Impact of ocean color on the maintenance of the Pacific Cold Tongue, *Geophys. Res. Lett.*, 34, L11609, doi:10.1029/2007GL030100, 2007. 3915
- Arakawa, A.: Computational design for long-term numerical integration of the equations of fluid motion: two-dimensional incompressible flow, Part 1., *J. Comput. Phys.*, 1, 119–143, 1966. 3897
- Babuska, I.: The finite-element method with Lagrangian multipliers, *Numer. Math.*, 20, 179–192, 1973. 3897
- Badia, S. and Codina, R.: Analysis of a stabilized finite element approximation of the transient convection-diffusion equation using an ALE framework, *Siam J. Numer. Anal.*, 44, 2159–2197, 2006. 3934
- Ballabrera-Poy, J., Murtugudde, R., Zhang, R. H., and Busalacchi, A. J.: Coupled ocean-atmosphere response to seasonal modulation of ocean color: impact on interannual climate simulations in the tropical Pacific, *J. Climate*, 20, 353–374, 2007. 3916
- Barnier, B., Madec, G., Penduff, T., Molines, J.-M., Treguier, A.-M., Le Sommer, J., Beckmann, A., Biastoch, A., Boening, C., Dengg, J., Derval, C., Durand, E., Gulev, S., Remy, E., Talandier, C., Theetten, S., Maltrud, M., McClean, J., and De Cuevas, B.: Impact of partial steps and momentum advection schemes in a global ocean circulation model at eddy-permitting resolution, *Ocean Dynam.*, 56, 543–567, 2006. 3904
- Bauer, S., Swenson, M. S., Griffa, A., Mariano, A. J., and Owens, K.: Eddy mean flow decomposition and eddy-diffusivity estimates in the tropical Pacific Ocean 1. Methodology, *J. Geophys. Res.-Oceans*, 103, 30855–30871, 1998. 3926

GMDD

6, 3893–3976, 2013

The Finite Element Sea ice-Ocean Model (FESOM)

Q. Wang et al.

Title Page

Abstract

Introduction

Conclusions

References

Tables

Figures

◀

▶

◀

▶

Back

Close

Full Screen / Esc

Printer-friendly Version

Interactive Discussion



The Finite Element Sea ice-Ocean Model (FESOM)

Q. Wang et al.

Title Page

Abstract

Introduction

Conclusions

References

Tables

Figures



Back

Close

Full Screen / Esc

Printer-friendly Version

Interactive Discussion



- Beckmann, A. and Döscher, R.: A method for improved representation of dense water spreading over topography in geopotential-coordinate models, *J. Phys. Oceanogr.*, 27, 581–591, 1997. 3937
- 5 Beckmann, A. and Haidvogel, D. B.: Numerical-simulation of flow around a tall isolated seamount, 1. Problem formulation and model accuracy, *J. Phys. Oceanogr.*, 23, 1736–1753, 1993. 3907
- Böning, C., Timmermann, R., Macrander, A., and Schröter, J.: A pattern-filtering method for the determination of ocean bottom pressure anomalies from GRACE solutions, *Geophys. Res. Lett.*, 35, L18611, doi:10.1029/2008GL034974, 2008. 3929
- 10 Boning, C. W., Holland, W. R., Bryan, F. O., Danabasoglu, G., and McWilliams, J. C.: An overlooked problem in model simulations of the thermohaline circulation and heat-transport in the Atlantic-ocean, *J. Climate*, 8, 515–523, 1995. 3922
- Brezzi, F.: On the existence, uniqueness and approximation of saddle-point problems arising from lagrangian multipliers, *ESAIM: Mathematical Modelling and Numerical Analysis – Modélisation Mathématique et Analyse Numérique*, 8, 129–151, 1974. 3897
- 15 Bryan, F.: Parameter sensitivity of primitive equation ocean general-circulation models, *J. Phys. Oceanogr.*, 17, 970–985, 1987. 3909
- Bryan, F. O., Hecht, M. W., and Smith, R. D.: Resolution convergence and sensitivity studies with North Atlantic circulation models, Part I: The western boundary current system, *Ocean Model.*, 16, 141–159, 2007. 3918, 3921
- 20 Bryan, K. and Lewis, L. J.: Water mass model of the World Ocean, *J. Geophys. Res.-Oceans*, 84, 2503–2517, 1979. 3912, 3914
- Bryan, K., Manabe, S., and Pacanowski, R. C.: Global Ocean-atmosphere climate model, 2. Oceanic circulation, *J. Phys. Oceanogr.*, 5, 30–46, 1975. 3917, 3918
- 25 Bryan, K., Dukowicz, J. K., and Smith, R. D.: On the mixing coefficient in the parameterization of bolus velocity, *J. Phys. Oceanogr.*, 29, 2442–2456, 1999. 3926
- Campin, J.-M., Marshall, J., and Ferreira, D.: Sea ice-ocean coupling using a rescaled vertical coordinate z^* , *Ocean Model.*, 24, 1–14, 2008. 3934
- Campin, J.-M., Hill, C., Jones, H., and Marshall, J.: Super-parameterization in ocean modeling: application to deep convection, *Ocean Model.*, 36, 90–101, 2011. 3917
- 30 Chassignet, E. P. and Garraffo, Z. D.: Viscosity parameterization and the Gulf Stream separation, in: Proceedings “Aha Huliko” a Hawaiian Winter Workshop, 16–19 January 2001, University of Hawaii, edited by: Muller, P. and Henderson, D., 39–43, 2001. 3921

The Finite Element Sea ice-Ocean Model (FESOM)

Q. Wang et al.

Title Page

Abstract

Introduction

Conclusions

References

Tables

Figures

⏪

⏩

◀

▶

Back

Close

Full Screen / Esc

Printer-friendly Version

Interactive Discussion



- Chassignet, E. P. and Marshall, D. P.: Gulf Stream separation in numerical ocean models, in: Ocean Modeling in an Eddy Regime, edited by: Hecht, M. W. and Hasumi, H., AGU, Washington, D.C., Geophys. Monogr. Ser., 177, 39–61, 2008. 3921
- Chassignet, E. P., Arango, H., Dietrich, D., Ezer, T., Ghil, M., Haidvogel, D. B., Ma, C. C., Mehra, A., Paiva, A. M., and Sirkes, Z.: DAMEE-NAB: the base experiments, Dyn. Atmos. Oceans, 32, 155–183, 2000. 3903
- Chen, C., Liu, H., and Beardsley, R. C.: An unstructured, finite volume, three-dimensional, primitive equation ocean model: application to coastal ocean and estuaries, J. Atmos. Ocean. Tech., 20, 159–186, 2003. 3895
- Codina, R. and Soto, O.: Finite element solution of the Stokes problem with dominating Coriolis force, Comput. Method. Appl. M., 142, 215–234, 1997. 3897
- Cox, M. D.: A Primitive Equation Three-Dimensional Model of the Ocean, Tech. rep., Geophysical Fluid Dynamics Laboratory, Princeton University, USA, 1984. 3917
- Dai, A., Qian, T., Trenberth, K. E., and Milliman, J. D.: Changes in continental freshwater discharge from 1948 to 2004, J. Climate, 22, 2773–2792, 2009. 3931
- Danabasoglu, G. and Marshall, J.: Effects of vertical variations of thickness diffusivity in an ocean general circulation model, Ocean Model., 18, 122–141, 2007. 3926, 3927, 3928
- Danabasoglu, G. and McWilliams, J. C.: Sensitivity of the global ocean circulation to parameterizations of mesoscale tracer transports, J. Climate, 8, 2967–2987, 1995. 3923, 3924, 3926
- Danabasoglu, G., McWilliams, J. C., and Gent, P. R.: The role of mesoscale tracer transports in the global ocean circulation, Science, 264, 1123–1126, 1994. 3923
- Danabasoglu, G., Large, W. G., Tribbia, J. J., Gent, P. R., Briegleb, B. P., and McWilliams, J. C.: Diurnal coupling in the tropical oceans of CCSM3, J. Climate, 19, 2347–2365, 2006. 3910, 3926, 3931
- Danabasoglu, G., Ferrari, R., and McWilliams, J. C.: Sensitivity of an ocean general circulation model to a parameterization of near-surface eddy fluxes, J. Climate, 21, 1192–1208, 2008. 3924, 3925
- Danabasoglu, G., Large, W. G., and Briegleb, B. P.: Climate impacts of parameterized Nordic Sea overflows, J. Geophys. Res., 115, C11005, doi:10.1029/2010JC006243, 2010. 3937
- Danabasoglu, G., Bates, S. C., Briegleb, B. P., Jayne, S. R., Jochum, M., Large, W. G., Peacock, S., and Yeager, S. G.: The CCSM4 ocean component, J. Climate, 25, 1361–1389, 2012. 3913, 3914, 3927

The Finite Element Sea ice-Ocean Model (FESOM)

Q. Wang et al.

Title Page

Abstract

Introduction

Conclusions

References

Tables

Figures



Back

Close

Full Screen / Esc

Printer-friendly Version

Interactive Discussion



- Danabasoglu, G., Yeager, S. G., Bailey, D., Behrens, E., Bentsen, M., Bi, D., Biastoch, A., Boening, C., Bozec, A., Canuto, V. M., Cassou, C., Chassignet, E., Coward, A. C., Danilov, S., Diansky, N., Drange, H., Farneti, R., Fernandez, E., Fogli, P. G., Forget, G., Fujii, Y., Griffies, S. M., Gusev, A., Heimbach, P., Howard, A., Jung, T., Kelley, M., Large, W. G., Leboissetier, A., Lu, J., Madec, G., Marsland, S. J., Masina, S., Navarra, A., Nurser, A. J. G., Pirani, A., Salasy Melia, D., Samuels, B. L., Scheinert, M., Sidorenko, D., Treguier, A.-M., Tsujino, H., Uotila, P., Valcke, S., Voldoire, A., and Wang, Q.: North Atlantic simulated in Coordinated Ocean-ice Reference Experiments phase II (CORE-II), Part I: Mean states, Ocean Model., submitted, 2013. 3934, 3937
- 5 Danilov, S., Kivman, G., and Schröter, J.: A finite-element ocean model: principles and evaluation, Ocean Model., 6, 125–150, 2004. 3895, 3897, 3899, 3900, 3934
- Danilov, S., Wang, Q., Losch, M., Sidorenko, D., and Schröter, J.: Modeling ocean circulation on unstructured meshes: comparison of two horizontal discretizations, Ocean Dynam., 58, 365–374, 2008. 3900
- 10 de Jong, M. F., van Aken, H. M., Vage, K., and Pickart, R. S.: Convective mixing in the central Irminger Sea: 2002–2010, Deep-Sea Res. I, 63, 36–51, 2012. 3920
- Delworth, T. L., Rosati, A., Anderson, W., Adcroft, A. J., Balaji, V., Benson, R., Dixon, K., Griffies, S. M., Lee, H.-C., Pacanowski, R. C., Vecchi, G. A., Wittenberg, A. T., Zeng, F., and Zhang, R.: Simulated climate and climate change in the GFDL CM2.5 high-resolution coupled climate model, J. Climate, 25, 2755–2781, 2012. 3914, 3922
- 20 Doos, K. and Webb, D. J.: The Deacon Cell and the other meridional cells of the Southern ocean, J. Phys. Oceanogr., 24, 429–442, 1994. 3929
- Duffy, P. B., Eltgroth, P., Bourgeois, A. J., and Caldeira, K.: Effect of improved subgrid scale transport of tracers on uptake of bomb radiocarbon in the GFDL ocean general-circulation model, Geophys. Res. Lett., 22, 1065–1068, 1995. 3923
- 25 Duffy, P. B., Caldeira, K., Selvaggi, J., and Hoffert, M. I.: Effects of subgrid-scale mixing parameterizations on simulated distributions of natural C-14, temperature, and salinity in a three-dimensional ocean general circulation model, J. Phys. Oceanogr., 27, 498–523, 1997. 3923
- Dunne, J. P., John, J. G., Adcroft, A. J., Griffies, S. M., Hallberg, R. W., Shevliakova, E., Stouffer, R. J., Cooke, W., Dunne, K. A., Harrison, M. J., Krasting, J. P., Malyshev, S. L., Milly, P. C. D., Phillipps, P. J., Sentman, L. T., Samuels, B. L., Spelman, M. J., Winton, M., Wittenberg, A. T., and Zadeh, N.: GFDL's ESM2 global coupled climate-carbon earth system
- 30

The Finite Element Sea ice-Ocean Model (FESOM)

Q. Wang et al.

Title Page

Abstract

Introduction

Conclusions

References

Tables

Figures

◀

▶

◀

▶

Back

Close

Full Screen / Esc

Printer-friendly Version

Interactive Discussion



models, part I: physical formulation and baseline simulation characteristics, *J. Climate*, 25, 6646–6665, 2012. 3914, 3918

Durran, D. R.: Numerical Methods for Wave Equations in Geophysical Fluid Dynamics, Springer, 1999. 3898

5 Eden, C.: Thickness diffusivity in the Southern Ocean, *Geophys. Res. Lett.*, 33, L11606, doi:10.1029/2006GL026157, 2006. 3926

Eden, C. and Greatbatch, R. J.: Towards a mesoscale eddy closure, *Ocean Model.*, 20, 223–239, 2008. 3926, 3930

10 Eden, C. and Willebrand, J.: Mechanism of interannual to decadal variability of the North Atlantic circulation, *J. Climate*, 14, 2266–2280, 2001. 3907

Eden, C., Greatbatch, R. J., and Willebrand, J.: A diagnosis of thickness fluxes in an eddy-resolving model, *J. Phys. Oceanogr.*, 37, 727–742, 2007. 3926

Eden, C., Jochum, M., and Danabasoglu, G.: Effects of different closures for thickness diffusivity, *Ocean Model.*, 26, 47–59, 2009. 3926

15 England, M. H.: Using Chlorofluorocarbons to assess ocean climate models, *Geophys. Res. Lett.*, 22, 3051–3054, 1995. 3923

England, M. H. and Hirst, A. C.: Chlorofluorocarbon uptake in a World Ocean model: 2. Sensitivity to surface thermohaline forcing and subsurface mixing parameterizations, *J. Geophys. Res.-Oceans*, 102, 15709–15731, 1997. 3923

20 Exarchou, E., von Storch, J.-S., and Jungclauss, J. H.: Sensitivity of transient climate change to tidal mixing: Southern Ocean heat uptake in climate change experiments performed with ECHAM5/MPIOM, *Clim. Dynam.*, online first, doi:10.1007/s00382-013-1776-y, 2013. 3914

Ezer, T. and Mellor, G. L.: A generalized coordinate ocean model and a comparison of the bottom boundary layer dynamics in terrain-following and in z-level grids, *Ocean Model.*, 6, 379–403, 2004. 3904

25 Fahrbach, E., Rohardt, G., Schröder, M., and Strass, V.: Transport and structure of the Weddell Gyre, *Ann. Geophys.*, 12, 840–855, doi:10.1007/s00585-994-0840-7, 1994. 3907

Farhat, C., Geuzaine, P., and Grandmont, C.: The discrete geometric conservation law and the nonlinear stability of ALE schemes for the solution of flow problems on moving grids, *J. Comput. Phys.*, 174, 669–694, 2001. 3934

30 Farneti, R. and Gent, P. R.: The effects of the eddy-induced advection coefficient in a coarse-resolution coupled climate model, *Ocean Model.*, 39, 135–145, 2011. 3928, 3929, 3930

The Finite Element Sea ice-Ocean Model (FESOM)

Q. Wang et al.

Title Page

Abstract

Introduction

Conclusions

References

Tables

Figures

◀

▶

◀

▶

Back

Close

Full Screen / Esc

Printer-friendly Version

Interactive Discussion



- Farneti, R., Delworth, T. L., Rosati, A. J., Griffies, S. M., and Zeng, F.: The Role of mesoscale eddies in the rectification of the Southern Ocean response to climate change, *J. Phys. Oceanogr.*, 40, 1539–1557, 2010. 3922, 3928, 3929
- 5 Fer, I.: Weak vertical diffusion allows maintenance of cold halocline in the central Arctic, *Atmospheric and Oceanic Science Letters (AOSL)*, 2, 148–152, 2009. 3913, 3914
- Ferrari, R., McWilliams, J., Canuto, V., and Dubovikov, M.: Parameterization of eddy fluxes near oceanic boundaries, *J. Climate*, 21, 2770–2789, 2008. 3925
- Ferrari, R., Griffies, S. M., Nurser, A. J. G., and Vallis, G. K.: A boundary-value problem for the parameterized mesoscale eddy transport, *Ocean Model.*, 32, 143–156, 2010. 3930
- 10 Ferreira, D. and Marshall, J.: Formulation and implementation of a “residual-mean” ocean circulation model, *Ocean Model.*, 13, 86–107, 2006. 3926, 3927
- Ferreira, D., Marshall, J., and Heimbach, P.: Estimating eddy stresses by fitting dynamics to observations using a residual-mean ocean circulation model and its adjoint, *J. Phys. Oceanogr.*, 35, 1891–1910, 2005. 3926, 3927
- 15 Fischer, J., Schott, F. A., and Dengler, M.: Boundary circulation at the exit of the Labrador Sea, *J. Phys. Oceanogr.*, 34, 1548–1570, 2004. 3907
- Fischer, J., Visbeck, M., Zantopp, R., and Nunes, N.: Interannual to decadal variability of outflow from the Labrador Sea, *Geophys. Res. Lett.*, 37, L24610, doi:10.1029/2010GL045321, 2010. 3907
- 20 Formaggia, L. and Nobile, F.: Stability analysis of second-order time accurate schemes for ALE-FEM, *Comput. Method. Appl. M.*, 193, 4097–4116, 2004. 3934
- Fretwell, P., Pritchard, H. D., Vaughan, D. G., Bamber, J. L., Barrand, N. E., Bell, R., Bianchi, C., Bingham, R. G., Blankenship, D. D., Casassa, G., Catania, G., Callens, D., Conway, H., Cook, A. J., Corr, H. F. J., Damaske, D., Damm, V., Ferraccioli, F., Forsberg, R., Fujita, S.,
- 25 Gim, Y., Gogineni, P., Griggs, J. A., Hindmarsh, R. C. A., Holmlund, P., Holt, J. W., Jacobel, R. W., Jenkins, A., Jokat, W., Jordan, T., King, E. C., Kohler, J., Krabill, W., Riger-Kusk, M., Langlely, K. A., Leitchenkov, G., Leuschen, C., Luyendyk, B. P., Matsuoka, K., Mouginit, J., Nitsche, F. O., Nogi, Y., Nost, O. A., Popov, S. V., Rignot, E., Rippin, D. M., Rivera, A., Roberts, J., Ross, N., Siegert, M. J., Smith, A. M., Steinhage, D., Studinger, M.,
- 30 Sun, B., Tinto, B. K., Welch, B. C., Wilson, D., Young, D. A., Xiangbin, C., and Zirizzotti, A.: Bedmap2: improved ice bed, surface and thickness datasets for Antarctica, *The Cryosphere*, 7, 375–393, doi:10.5194/tc-7-375-2013, 2013. 3906

The Finite Element Sea ice-Ocean Model (FESOM)

Q. Wang et al.

Title Page

Abstract

Introduction

Conclusions

References

Tables

Figures

⏪

⏩

◀

▶

Back

Close

Full Screen / Esc

Printer-friendly Version

Interactive Discussion



- Fringer, O. B., Gerritsen, M., and Street, R. L.: An unstructured-grid, finite-volume, nonhydrostatic, parallel coastal ocean simulator, *Ocean Model.*, 14, 139–173, 2006. 3895
- Gent, P. R. and Danabasoglu, G.: Response to increasing Southern Hemisphere winds in CCSM4, *J. Climate*, 24, 4992–4998, 2011. 3929
- 5 Gent, P. R. and McWilliams, J. C.: Isopycnal mixing in ocean circulation models, *J. Phys. Oceanogr.*, 20, 150–155, 1990. 3923
- Gent, P. R., Willebrand, J., McDougall, T. J., and McWilliams, J. C.: Parameterizing eddy-induced tracer transports in ocean circulation models, *J. Phys. Oceanogr.*, 25, 463–474, 1995. 3923
- 10 Gent, P. R., Bryan, F. O., Danabasoglu, G., Doney, S. C., Holland, W. R., Large, W. G., and McWilliams, J. C.: The NCAR Climate System Model global ocean component, *J. Climate*, 11, 1287–1306, 1998. 3910
- Gerdes, R., Köberle, C., and Willebrand, J.: The influence of numerical advection schemes on the results of ocean general circulation models, *Clim. Dynam.*, 5, 211–226, 1991. 3926
- 15 Glessmer, M. S., Oschlies, A., and Yool, A.: Simulated impact of double-diffusive mixing on physical and biogeochemical upper ocean properties, *J. Geophys. Res.*, 113, C08029, doi:10.1029/2007JC004455, 2008. 3910
- Gnanadesikan, A., Griffies, S. M., and Samuels, B. L.: Effects in a climate model of slope tapering in neutral physics schemes, *Ocean Model.*, 16, 1–16, 2007. 3930
- 20 Gnanadesikan, A., Emanuel, K., Vecchi, G. A., Anderson, W. G., and Hallberg, R.: How ocean color can steer Pacific tropical cyclones, *Geophys. Res. Lett.*, 37, L18802, doi:10.1029/2010GL044514, 2010. 3916
- Gregg, M. C., Sanford, T. B., and Winkel, D. P.: Reduced mixing from the breaking of internal waves in equatorial waters, *Nature*, 422, 513–515, 2003. 3912
- 25 Griffies, S.: Elements of the Modular Ocean Model (MOM) 2012 release, Tech. rep., GFDL, Princeton, USA, 2012. 3911
- Griffies, S. M.: The Gent–McWilliams skew flux, *J. Phys. Oceanogr.*, 28, 831–841, 1998. 3923
- Griffies, S. M.: *Fundamentals of Ocean Climate Models*, Princeton University Press, Princeton and Oxford, 2004. 3894, 3903, 3918, 3922, 3924, 3925, 3928, 3937
- 30 Griffies, S. M. and Hallberg, R. W.: Biharmonic friction with a Smagorinsky-like viscosity for use in large-scale eddy-permitting ocean models, *Mon. Weather Rev.*, 128, 2935–2946, 2000. 3909, 3918, 3919, 3928

The Finite Element Sea ice-Ocean Model (FESOM)

Q. Wang et al.

Title Page

Abstract

Introduction

Conclusions

References

Tables

Figures

◀

▶

◀

▶

Back

Close

Full Screen / Esc

Printer-friendly Version

Interactive Discussion



- Griffies, S. M., Gnanadesikan, A., Pacanowski, R. C., Larichev, V. D., Dukowicz, J. K., and Smith, R. D.: Isonutral diffusion in a z-coordinate ocean model, *J. Phys. Oceanogr.*, 28, 805–830, 1998. 3922, 3923
- Griffies, S. M., Pacanowski, R. C., and Hallberg, R. W.: Spurious diapycnal mixing associated with advection in a z-coordinate ocean model, *Mon. Weather Rev.*, 128, 538–564, 2000. 3903, 3917
- Griffies, S. M., Gnanadesikan, A., Dixon, K. W., Dunne, J. P., Gerdes, R., Harrison, M. J., Rosati, A., Russell, J. L., Samuels, B. L., Spelman, M. J., Winton, M., and Zhang, R.: Formulation of an ocean model for global climate simulations, *Ocean Sci.*, 1, 45–79, doi:10.5194/os-1-45-2005, 2005. 3911, 3916, 3918, 3924, 3925, 3926, 3931
- Griffies, S. M., Biastoch, A., Böning, C., Bryan, F., Danabasoglu, G., Chassignet, E. P., England, M. H., Gerdes, R., Haak, H., Hallberg, R. W., Hazeleger, W., Jungclaus, J., Large, W. G., Madec, G., Pirani, A., Samuels, B. L., Scheinert, M., Gupta, A. S., Severijns, C. A., Simmons, H. L., Treguier, A. M., Winton, M., Yeager, S., and Yin, J.: Coordinated Ocean-ice Reference Experiments (COREs), *Ocean Model.*, 26, 1–46, 2009. 3937
- Haidvogel, D. B. and Beckmann, A.: *Numerical Ocean Circulation Modeling*, Imperial College Press, London, 1999. 3903
- Hallberg, R. and Gnanadesikan, A.: The role of eddies in determining the structure and response of the wind-driven Southern Hemisphere overturning: results from the Modeling Eddies in the Southern Ocean (MESO) project, *J. Phys. Oceanogr.*, 36, 2232–2252, 2006. 3929
- Haney, R. L.: On the pressure-gradient force over steep topography in sigma coordinate ocean models, *J. Phys. Oceanogr.*, 21, 610–619, 1991. 3907
- Hecht, M. W., Petersen, M. R., Wingate, B. A., Hunke, E., and Maltrud, M.: Lateral mixing in the eddying regime and a new broad-ranging formulation, in: *Ocean Modeling in an Eddying Regime*, edited by: Hecht, M. W. and Hasumi, H., *Geophys. Monogr. Ser. vol. 177*, AGU, Washington, D.C., 2008. 3918
- Held, I. M. and Larichev, V. D.: A scaling theory for horizontally homogeneous, baroclinically unstable flow on a beta plane, *J. Atmos. Sci.*, 53, 946–952, 1996. 3926
- Hellmer, H. H. and Olbers, D. J.: A 2-dimensional model for the thermohaline circulation under an ice shelf, *Antarct. Sci.*, 1, 325–336, 1989. 3935
- Hellmer, H. H., Kauker, F., Timmermann, R., Determann, J., and Rae, J.: Twenty-first-century warming of a large Antarctic ice-shelf cavity by a redirected coastal current, *Nature*, 485, 225–228, 2012. 3937

The Finite Element Sea ice-Ocean Model (FESOM)

Q. Wang et al.

Title Page

Abstract

Introduction

Conclusions

References

Tables

Figures

◀

▶

◀

▶

Back

Close

Full Screen / Esc

Printer-friendly Version

Interactive Discussion



- Hibiya, T., Nagasawa, M., and Niwa, Y.: Latitudinal dependence of diapycnal diffusivity in the thermocline observed using a microstructure profiler, *Geophys. Res. Lett.*, 34, L24602, doi:10.1029/2007GL032323, 2007. 3913
- 5 Hirst, A. C. and McDougall, T. J.: Deep-water properties and surface buoyancy flux as simulated by a z-coordinate model including eddy-induced advection, *J. Phys. Oceanogr.*, 26, 1320–1343, 1996. 3923
- Hirst, A. C. and McDougall, T. J.: Meridional overturning and dianeutral transport in a z-coordinate ocean model including eddy-induced advection, *J. Phys. Oceanogr.*, 28, 1205–1223, 1998. 3923
- 10 Hirst, A. C., O’Farrell, S. P., and Gordon, H. B.: Comparison of a coupled ocean-atmosphere model with and without oceanic eddy-induced advection, Part I: Ocean spinup and control integrations, *J. Climate*, 13, 139–163, 2000. 3923
- Holland, D. M. and Jenkins, A.: Modeling thermodynamic ice-ocean interactions at the base of an ice shelf, *J. Phys. Oceanogr.*, 29, 1787–1800, 1999. 3935
- 15 Holloway, G. and Wang, Z.: Representing eddy stress in an Arctic Ocean model, *J. Geophys. Res.*, 114, C06020, doi:10.1029/2008JC005169, 2009. 3927
- Huang, R. X.: Mixing and energetics of the oceanic thermohaline circulation, *J. Phys. Oceanogr.*, 29, 727–746, 1999. 3912
- Ilicak, M., Adcroft, A. J., Griffies, S. M., and Hallberg, R. W.: Spurious dianeutral mixing and the role of momentum closure, *Ocean Model.*, 45–46, 37–58, 2012. 3909
- Jahn, A., Aksenov, Y., de Cuevas, B. A., de Steur, L., Hakkinen, S., Hansen, E., Herbaut, C., Houssais, M. N., Karcher, M., Kauker, F., Lique, C., Nguyen, A., Pemberton, P., Worthen, D., and Zhang, J.: Arctic Ocean freshwater: how robust are model simulations?, *J. Geophys. Res.*, 117, C00D16, doi:10.1029/2012JC007907, 2012. 3902, 3911, 3913
- 25 Jakob, C.: Accelerating progress in global atmospheric model development through improved parametrizations, *B. Am. Meteorol. Soc.*, 91, 869–875, 2010. 3894
- Jakobsson, M., Macnab, R., Mayer, L., Anderson, R., Edwards, M., Hatzky, J., Schenke, H. W., and Johnson, P.: An improved bathymetric portrayal of the Arctic Ocean: implications for ocean modeling and geological, geophysical and oceanographic analyses, *Geophys. Res. Lett.*, 35, L07602, doi:10.1029/2008GL033520, 2008. 3905
- 30 Jakobsson, M., Mayer, L., Coakley, B., Dowdeswell, J. A., Forbes, S., Fridman, B., Hodnesdal, H., Noormets, R., Pedersen, R., Rebesco, M., Schenke, H. W., Zarayskaya, Y., Accettella, D., Armstrong, A., Anderson, R. M., Bienhoff, P., Camerlenghi, A., Church, I., Ed-

The Finite Element Sea ice-Ocean Model (FESOM)

Q. Wang et al.

Title Page

Abstract

Introduction

Conclusions

References

Tables

Figures

⏪

⏩

◀

▶

Back

Close

Full Screen / Esc

Printer-friendly Version

Interactive Discussion



wards, M., Gardner, J. V., Hall, J. K., Hell, B., Hestvik, O., Kristoffersen, Y., Marcussen, C., Mohammad, R., Mosher, D., Nghiem, S. V., Teresa Pedrosa, M., Travaglini, P. G., and Weatherall, P.: The International Bathymetric Chart of the Arctic Ocean (IBCAO) Version 3.0, *Geophys. Res. Lett.*, 39, L12609, doi:10.1029/2012GL052219, 2012. 3906

5 Jayne, S. R.: The impact of abyssal mixing parameterizations in an ocean general circulation model, *J. Phys. Oceanogr.*, 39, 1756–1775, 2009. 3914

Jenkins, A.: A one-dimensional model of ice shelf-ocean interaction, *J. Geophys. Res.*, 96, 20671–20677, doi:10.1029/91JC01842, 1991. 3935

Jochum, M.: Impact of latitudinal variations in vertical diffusivity on climate simulations, *J. Geophys. Res.*, 114, C01010, doi:10.1029/2008JC005030, 2009. 3909

10 Jochum, M., Danabasoglu, G., Holland, M., Kwon, Y. O., and Large, W. G.: Ocean viscosity and climate, *J. Geophys. Res.*, 113, C06017, doi:10.1029/2007JC004515, 2008. 3913, 3920, 3921

Jochum, M., Yeager, S., Lindsay, K., Moore, K., and Murtugudde, R.: Quantification of the feedback between phytoplankton and ENSO in the community climate system model, *J. Climate*, 23, 2916–2925, 2010. 3916

Jochum, M., Briegleb, B. P., Danabasoglu, G., Large, W. G., Norton, N. J., Jayne, S. R., Alford, M. H., and Bryan, F. O.: The impact of oceanic near-inertial waves on climate, *J. Climate*, 26, 2833–2844, 2013. 3913, 3915

20 Jones, D. C., Ito, T., and Lovenduski, N. S.: The transient response of the Southern Ocean pycnocline to changing atmospheric winds, *Geophys. Res. Lett.*, 38, L15604, doi:10.1029/2011GL048145, 2011. 3929

Jungclaus, J., Fischer, N., Haak, H., Lohmann, K., Marotzke, J., Matei, D., Mikolajewicz, U., Notz, D., and von Storch, J.: Characteristics of the ocean simulations in MPIOM, the ocean component of the MPI-Earth System Model, *J. Adv. Model. Earth Syst.*, 5, doi:10.1002/jame.20023, online first, 2013. 3910

25 Karcher, M., Kauker, F., Gerdes, R., Hunke, E., and Zhang, J.: On the dynamics of Atlantic Water circulation in the Arctic Ocean, *J. Geophys. Res.*, 112, C04S02, doi:10.1029/2006JC003630, 2007. 3913

30 Kelley, D. E. and Van Scoy, K. A.: A basinwide estimate of vertical mixing in the upper pycnocline: spreading of bomb tritium in the North Pacific Ocean, *J. Phys. Oceanogr.*, 29, 1759–1771, 1999. 3912

The Finite Element Sea ice-Ocean Model (FESOM)

Q. Wang et al.

Title Page

Abstract

Introduction

Conclusions

References

Tables

Figures

◀

▶

◀

▶

Back

Close

Full Screen / Esc

Printer-friendly Version

Interactive Discussion



- Killworth, P. D.: On the parameterization of eddy transfer, Part I. Theory, *J. Mar. Res.*, 55, 1171–1197, 1997. 3926
- Klinger, B. A., Marshall, J., and Send, U.: Representation of convective plumes by vertical adjustment, *J. Geophys. Res.-Oceans*, 101, 18175–18182, 1996. 3917
- 5 Ladyzhenskaya, O.: *Mathematical Theory of Viscous Incompressible Flows*, Gordon and Breach Science Publishers, New York, 1969. 3897
- Large, W. G. and Yeager, S. G.: The global climatology of an interannually varying air-sea flux data set, *Clim. Dynam.*, 33, 341–364, 2009. 3901
- 10 Large, W. G., McWilliams, J. C., and Doney, S. C.: Oceanic vertical mixing – a review and a model with a nonlocal boundary-layer parameterization, *Rev. Geophys.*, 32, 363–403, 1994. 3909, 3910
- Large, W. G., Danabasoglu, G., Doney, S. C., and McWilliams, J. C.: Sensitivity to surface forcing and boundary layer mixing in a global ocean model: annual-mean climatology, *J. Phys. Oceanogr.*, 27, 2418–2447, 1997. 3910, 3924, 3925
- 15 Large, W. G., Danabasoglu, G., McWilliams, J. C., Gent, P. R., and Bryan, F. O.: Equatorial circulation of a global ocean climate model with anisotropic horizontal viscosity, *J. Phys. Oceanogr.*, 31, 518–536, 2001. 3917, 3918
- Latif, M., Anderson, D., Barnett, T., Cane, M., Kleeman, R., Leetmaa, A., O'Brien, J., Rosati, A., and Schneider, E.: A review of the predictability and prediction of ENSO, *J. Geophys. Res.-Oceans*, 103, 14375–14393, 1998. 3902
- 20 Laurent, L. S., Garabato, A. C. N., Ledwell, J. R., Thurnherr, A. M., Toole, J. M., and Watson, A. J.: Turbulence and diapycnal mixing in Drake Passage, *J. Phys. Oceanogr.*, 42, 2143–2152, 2012. 3912
- Ledwell, J. R., Watson, A. J., and Law, C. S.: Evidence for slow mixing across the pycnocline from an open-ocean tracer-release experiment, *Nature*, 364, 701–703, 1993. 3912
- 25 Ledwell, J. R., Watson, A. J., and Law, C. S.: Mixing of a tracer in the pycnocline, *J. Geophys. Res.-Oceans*, 103, 21499–21529, 1998. 3912, 3926
- Ledwell, J. R., Montgomery, E. T., Polzin, K. L., St Laurent, L. C., Schmitt, R. W., and Toole, J. M.: Evidence for enhanced mixing over rough topography in the abyssal ocean, *Nature*, 403, 179–182, 2000. 3912
- 30 Lee, H. C., Rosati, A., and Spelman, M. J.: Barotropic tidal mixing effects in a coupled climate model: oceanic conditions in the Northern Atlantic, *Ocean Model.*, 11, 464–477, 2006. 3910, 3911, 3914, 3931

The Finite Element Sea ice-Ocean Model (FESOM)

Q. Wang et al.

Title Page

Abstract

Introduction

Conclusions

References

Tables

Figures



Back

Close

Full Screen / Esc

Printer-friendly Version

Interactive Discussion



- Lengaigne, M., Madec, G., Bopp, L., Menkes, C., Aumont, O., and Cadule, P.: Bio-physical feedbacks in the Arctic Ocean using an Earth system model, *Geophys. Res. Lett.*, 36, L21602, doi:10.1029/2009GL040145, 2009. 3916
- Liu, H., Ma, J., Lin, P., and Zhan, H.: Numerical study of the effects of ocean color on the sea surface temperature in the southeast tropical Indian Ocean: the role of the barrier layer, *Environ. Res. Lett.*, 7, 024010, doi:10.1088/1748-9326/7/2/024010, 2012. 3916
- Loeptien, U., Eden, C., Timmermann, A., and Dietze, H.: Effects of biologically induced differential heating in an eddy-permitting coupled ocean-ecosystem model, *J. Geophys. Res.*, 114, C06011, doi:10.1029/2008JC004936, 2009. 3916
- Löhner, R., Morgan, K., Peraire, J., and Vahdati, M.: Finite-element flux-corrected transport (FEM-FCT) for the Euler and Navier–Stokes equations, *Int. J. Numer. Meth. Fl.*, 7, 1093–1109, 1987. 3908
- Losch, M.: Modeling ice shelf cavities in a z coordinate ocean general circulation model, *J. Geophys. Res.*, 113, C08043, doi:10.1029/2007JC004368, 2008. 3904
- Lytche, M. B., Vaughan, D. G., and the BEDMAP Consortium: BEDMAP: a new ice thickness and subglacial topographic model of Antarctica, *J. Geophys. Res.*, 106, 11335–11351, 2001. 3906
- Maier-Reimer, E., Mikolajewicz, U., and Hasselmann, K.: Mean circulation of the Hamburg LSG OGCM and its sensitivity to the thermohaline surface forcing, *J. Phys. Oceanogr.*, 23, 731–757, 1993. 3904
- Maltrud, M. and Holloway, G.: Implementing biharmonic neptune in a global eddying ocean model, *Ocean Model.*, 21, 22–34, 2008. 3927
- Marshall, D. P. and Adcroft, A. J.: Parameterization of ocean eddies: potential vorticity mixing, energetics and Arnold’s first stability theorem, *Ocean Model.*, 32, 188–204, 2010. 3930
- Marshall, J., Shuckburgh, E., Jones, H., and Hill, C.: Estimates and implications of surface eddy diffusivity in the Southern Ocean derived from tracer transport, *J. Phys. Oceanogr.*, 36, 1806–1821, 2006. 3926
- Marzeion, B., Timmermann, A., Murtugudde, R., and Jin, F. F.: Biophysical feedbacks in the tropical Pacific, *J. Climate*, 18, 58–70, 2005. 3915
- Mazloff, M. R., Heimbach, P., and Wunsch, C.: An eddy-permitting Southern Ocean state estimate, *J. Phys. Oceanogr.*, 40, 880–899, 2010. 3929
- McDougall, T. J.: Neutral surfaces, *J. Phys. Oceanogr.*, 17, 1950–1964, 1987. 3922

The Finite Element Sea ice-Ocean Model (FESOM)

Q. Wang et al.

Title Page

Abstract

Introduction

Conclusions

References

Tables

Figures

◀

▶

◀

▶

Back

Close

Full Screen / Esc

Printer-friendly Version

Interactive Discussion



- McGeehan, T. and Maslowski, W.: Impact of shelf basin freshwater transport on deep convection in the western Labrador Sea, *J. Phys. Oceanogr.*, 41, 2187–2210, 2011. 3931
- Meredith, M. P. and Hogg, A. M.: Circumpolar response of Southern Ocean eddy activity to a change in the southern annular mode, *Geophys. Res. Lett.*, 33, L16608, doi:10.1029/2006GL026499, 2006. 3929
- Meredith, M. P., Garabato, A. C. N., Hogg, A. M., and Farneti, R.: Sensitivity of the overturning circulation in the Southern Ocean to decadal changes in wind forcing, *J. Climate*, 25, 99–110, 2012. 3929
- Morel, A. and Antoine, D.: Heating rate within the upper ocean in relation to its biooptical state, *J. Phys. Oceanogr.*, 24, 1652–1665, 1994. 3916
- Morris, M. Y., Hall, M. M., St Laurent, L. C., and Hogg, N. G.: Abyssal mixing in the Brazil Basin, *J. Phys. Oceanogr.*, 31, 3331–3348, 2001. 3912
- Morrison, A. K. and Hogg, A. M.: On the relationship between Southern Ocean overturning and ACC transport, *J. Phys. Oceanogr.*, 43, 140–148, 2013. 3929, 3930
- Mueller, M., Haak, H., Jungclaus, J. H., Suendermann, J., and Thomas, M.: The effect of ocean tides on a climate model simulation, *Ocean Model.*, 35, 304–313, 2010. 3912
- Munday, D. R., Johnson, H. L., and Marshall, D. P.: Eddy saturation of equilibrated circumpolar currents, *J. Phys. Oceanogr.*, 43, 507–532, 2013. 3929, 3930
- Munk, W. and Wunsch, C.: Abyssal recipes II: energetics of tidal and wind mixing, *Deep-Sea Res. I*, 45, 1977–2010, 1998. 3912
- Munk, W. H.: On the wind-driven ocean circulation, *J. Meteorol.*, 7, 79–93, 1950. 3918
- Murtugudde, R., Beauchamp, J., McClain, C. R., Lewis, M., and Busalacchi, A. J.: Effects of penetrative radiation on the upper tropical ocean circulation, *J. Climate*, 15, 470–486, 2002. 3915, 3916
- Myers, P. G. and Deacu, D.: Labrador sea freshwater content in a model with a partial cell topographic representation, *Ocean Model.*, 6, 359–377, 2004. 3904
- Nakamoto, S., Kumar, S. P., Oberhuber, J. M., Ishizaka, J., Muneyama, K., and Frouin, R.: Response of the equatorial Pacific to chlorophyll pigment in a mixed layer isopycnal ocean general circulation model, *Geophys. Res. Lett.*, 28, 2021–2024, 2001. 3915
- Nguyen, A. T., Menemenlis, D., and Kwok, R.: Improved modeling of the Arctic halocline with a subgrid-scale brine rejection parameterization, *J. Geophys. Res.*, 114, C11014, doi:10.1029/2008JC005121, 2009. 3913, 3932

The Finite Element Sea ice-Ocean Model (FESOM)

Q. Wang et al.

Title Page

Abstract

Introduction

Conclusions

References

Tables

Figures

◀

▶

◀

▶

Back

Close

Full Screen / Esc

Printer-friendly Version

Interactive Discussion



- Nithiarasu, P.: An arbitrary Lagrangian Eulerian (ALE) formulation for free surface flows using the characteristic-based split (CBS) scheme, *Int. J. Numer. Meth. Fl.*, 48, 1415–1428, 2005. 3934
- Ohlmann, J. C.: Ocean radiant heating in climate models, *J. Climate*, 16, 1337–1351, 2003. 3916
- Olbers, D., Borowski, D., Volker, C., and Wolff, J. O.: The dynamical balance, transport and circulation of the Antarctic Circumpolar Current, *Antarct. Sci.*, 16, 439–470, 2004. 3907
- Olbers, D. J., Wenzel, M., and Willebrand, J.: The inference of north-atlantic circulation patterns from climatological hydrographic data, *Rev. Geophys.*, 23, 313–356, 1985. 3922
- Pacanowski, R. C. and Gnanadesikan, A.: Transient response in a z-level ocean model that resolves topography with partial cells, *Mon. Weather Rev.*, 126, 3248–3270, 1998. 3904
- Pacanowski, R. C. and Philander, S. G. H.: Parameterization of vertical mixing in numerical-models of tropical oceans, *J. Phys. Oceanogr.*, 11, 1443–1451, 1981. 3910
- Park, Y. G. and Bryan, K.: Comparison of thermally driven circulations from a depth-coordinate model and an isopycnal-layer model, part I: scaling-law sensitivity to vertical diffusivity, *J. Phys. Oceanogr.*, 30, 590–605, 2000. 3909
- Patara, L., Vichi, M., Masina, S., Fogli, P. G., and Manzini, E.: Global response to solar radiation absorbed by phytoplankton in a coupled climate model, *Clim. Dynam.*, 39, 1951–1968, 2012. 3916
- Persson, P. O. and Strang, G.: A simple mesh generator in MATLAB, *Siam Rev.*, 46, 329–345, 2004. 3901
- Pickart, R. S., Straneo, F., and Moore, G. W. K.: Is Labrador Sea water formed in the Irminger basin?, *Deep-Sea Res. Pt. I*, 50, 23–52, 2003. 3920
- Polzin, K. L., Toole, J. M., Ledwell, J. R., and Schmitt, R. W.: Spatial variability of turbulent mixing in the abyssal ocean, *Science*, 276, 93–96, 1997. 3912
- Rahmstorf, S.: A fast and complete convection scheme for ocean models, *Ocean Model.*, 101, 9–11, 1993. 3917
- Rainville, L. and Winsor, P.: Mixing across the Arctic ocean: microstructure observations during the Beringia 2005 expedition, *Geophys. Res. Lett.*, 35, L08606, doi:10.1029/2008GL033532, 2008. 3913
- Randall, D. A., Wood, R. A., Bony, S., Colman, R., Fichet, T., Fyfe, J., Kattsov, V., Pitman, A., Shukla, J., Srinivasan, J., Stouffer, R. J., Sumi, A., and Taylor, K. E.: Climate Models and Their Evaluation, in: *Climate Change 2007: The Physical Science Basis, Contribution of*

The Finite Element Sea ice-Ocean Model (FESOM)

Q. Wang et al.

Title Page

Abstract

Introduction

Conclusions

References

Tables

Figures

◀

▶

◀

▶

Back

Close

Full Screen / Esc

Printer-friendly Version

Interactive Discussion



Working Group I to the Fourth Assessment Report of the Intergovernmental Panel on Climate Change, edited by: Solomon, S., Qin, D., Manning, M., Chen, Z., Marquis, M., Averyt, K. B., Tignor, M., and Miller, H. L., Cambridge University Press, Cambridge, United Kingdom and New York, NY, USA, 2007. 3894

5 Redi, M. H.: Oceanic isopycnal mixing by coordinate rotation, *J. Phys. Oceanogr.*, 12, 1154–1158, 1982. 3922

Ringler, T., Petersen, M., Higdon, R., Jacobsen, D., Maltrud, M., and Jones, P. W.: A multi-resolution approach to Global Ocean Modeling, *Ocean Model.*, accepted, 2013. 3895

10 Roberts, M. and Marshall, D.: Do we require adiabatic dissipation schemes in eddy-resolving ocean models?, *J. Phys. Oceanogr.*, 28, 2050–2063, 1998. 3922, 3928

Robitaille, D. Y. and Weaver, A. J.: Validation of sub-grid-scale mixing schemes using cfc3 in a global ocean model, *Geophys. Res. Lett.*, 22, 2917–2920, 1995. 3923

15 Rochford, P. A., Kara, A. B., Wallcraft, A. J., and Arnone, R. A.: Importance of solar subsurface heating in ocean general circulation models, *J. Geophys. Res.-Oceans*, 106, 30923–30938, 2001. 3915

Saenko, O. A.: The effect of localized mixing on the ocean circulation and time-dependent climate change, *J. Phys. Oceanogr.*, 36, 140–160, 2006. 3914

20 Saenko, O. A., Zhai, X., Merryfield, W. J., and Lee, W. G.: The combined effect of tidally and eddy-driven diapycnal mixing on the large-scale ocean circulation, *J. Phys. Oceanogr.*, 42, 526–538, 2012. 3915

Schartau, M., Engel, A., Schröter, J., Thoms, S., Völker, C., and Wolf-Gladrow, D.: Modelling carbon overconsumption and the formation of extracellular particulate organic carbon, *Biogeosciences*, 4, 433–454, doi:10.5194/bg-4-433-2007, 2007. 3917

25 Schneider, E. K. and Zhu, Z. X.: Sensitivity of the simulated annual cycle of sea surface temperature in the equatorial Pacific to sunlight penetration, *J. Climate*, 11, 1932–1950, 1998. 3915

Schneider, E. K., DeWitt, D. G., Rosati, A., Kirtman, B. P., Ji, L., and Tribbia, J. J.: Retrospective ENSO forecasts: sensitivity to atmospheric model and ocean resolution, *Mon. Weather Rev.*, 131, 3038–3060, 2003. 3902

30 Scholz, P., Lohmann, G., Wang, Q., and Danilov, S.: Evaluation of a Finite-Element Sea-Ice Ocean Model (FESOM) set-up to study the interannual to decadal variability in the deep-water formation rates, *Ocean Dynam.*, 63, 347–370, 2013. 3901

The Finite Element Sea ice-Ocean Model (FESOM)

Q. Wang et al.

Title Page

Abstract

Introduction

Conclusions

References

Tables

Figures

◀

▶

◀

▶

Back

Close

Full Screen / Esc

Printer-friendly Version

Interactive Discussion



- Schroeder, M. and Fahrbach, E.: On the structure and the transport of the eastern Weddell Gyre, *Deep-Sea Res. Pt. II*, 46, 501–527, 1999. 3907
- Seny, B., Lambrechts, J., Comblen, R., Legat, V., and Remacle, J. F.: Multirate time stepping for accelerating explicit discontinuous Galerkin computations with application to geophysical flows, *Int. J. Numer. Meth. Fl.*, 71, 41–64, 2013. 3903
- Serreze, M. C., Barrett, A. P., Slater, A. G., Woodgate, R. A., Aagaard, K., Lammers, R. B., Steele, M., Moritz, R., Meredith, M., and Lee, C. M.: The large-scale freshwater cycle of the Arctic, *J. Geophys. Res.*, 111, C11010, doi:10.1029/2005JC003424, 2006. 3931
- Shchepetkin, A. F. and McWilliams, J. C.: A method for computing horizontal pressure-gradient force in an oceanic model with a nonaligned vertical coordinate, *J. Geophys. Res.*, 108, 3090, doi:10.1029/2001JC001047, 2003. 3908
- Shewchuk, J.: Triangle: Engineering a 2-D quality mesh generator and delaunay triangulator, in: *Applied Computational Geometry: Towards Geometric Engineering*, edited by: Lin, M. and Manocha, D., Springer-Verlag, Berlin, Lect. Notes Comput. Sc., 1148, 203–222, 1996. 3901
- Shukla, J., Hagedorn, R., Miller, M., Palmer, T., Hoskins, B., Kinter, J., Marotzke, J., and Slingo, J.: Strategies: revolution in climate prediction is both necessary and possible: a declaration at the world modelling summit for climate prediction, *B. Am. Meteorol. Soc.*, 90, 175–178, 2009. 3894
- Sidorenko, D., Wang, Q., Danilov, S., and Schroter, J.: FESOM under coordinated ocean-ice reference experiment forcing, *Ocean Dynam.*, 61, 881–890, 2011. 3901
- Sidorenko, D., Rackow, D., Barbi, D., Dorn, W., Jung, T., Semmler, T., Danilov, S., Dethlof, K., Goessling, H., Handorf, D., Harig, S., Hiller, W., Juricke, S., Schröter, J., Wang, Q., and Fieg, K.: Towards multi-resolution global climate modeling with ECHAM6-FESOM. Part I: Model formulation and mean climate, *Clim. Dynam.*, submitted, 2013. 3936
- Simmons, H. L., Jayne, S. R., St Laurent, L. C., and Weaver, A. J.: Tidally driven mixing in a numerical model of the ocean general circulation, *Ocean Model.*, 6, 245–263, 2004. 3914
- Smagorinsky, J.: General circulation experiments with the primitive equations: I. The basic experiment, *Mon. Weather Rev.*, 91, 99–164, 1963. 3919
- Smagorinsky, J.: Some historical remarks on the use of non-linear viscosities, in: *Large Eddy Simulation of Complex Engineering and Geophysical Flows*, edited by: Galperin, B. and Orszag, S. A., Cambridge University Press, Cambridge, 3–36, 1993. 3919
- Smith, R. D. and Gent, P. R.: Anisotropic Gent–McWilliams parameterization for ocean models, *J. Phys. Oceanogr.*, 34, 2541–2564, 2004. 3927

The Finite Element Sea ice-Ocean Model (FESOM)

Q. Wang et al.

Title Page

Abstract

Introduction

Conclusions

References

Tables

Figures

◀

▶

◀

▶

Back

Close

Full Screen / Esc

Printer-friendly Version

Interactive Discussion



- Smith, R. D. and McWilliams, J. C.: Anisotropic horizontal viscosity for ocean models, *Ocean Model.*, 5, 129–156, 2003. 3917, 3918
- Song, Y. H. and Haidvogel, D.: A semiimplicit ocean circulation model using a generalized topography-following coordinate system, *J. Comput. Phys.*, 115, 228–244, 1994. 3905
- 5 Song, Y. T.: A general pressure gradient formulation for ocean models, Part I: Scheme design and diagnostic analysis, *Mon. Weather Rev.*, 126, 3213–3230, 1998. 3908
- Song, Y. T. and Wright, D. G.: A general pressure gradient formulation for ocean models, Part II: Energy, momentum, and bottom torque consistency, *Mon. Weather Rev.*, 126, 3231–3247, 1998. 3908
- 10 St Laurent, L. C., Simmons, H. L., and Jayne, S. R.: Estimating tidally driven mixing in the deep ocean, *Geophys. Res. Lett.*, 29, 2106, doi:10.1029/2002GL015633, 2002. 3914
- Sundermeyer, M. A. and Price, J. F.: Lateral mixing and the North Atlantic Tracer Release Experiment: observations and numerical simulations of Lagrangian particles and a passive tracer, *J. Geophys. Res.-Oceans*, 103, 21481–21497, 1998. 3926
- 15 Sweeney, C., Gnanadesikan, A., Griffies, S. M., Harrison, M. J., Rosati, A. J., and Samuels, B. L.: Impacts of shortwave penetration depth on large-scale ocean circulation and heat transport, *J. Phys. Oceanogr.*, 35, 1103–1119, 2005. 3915, 3916, 3968
- Tian, J. W., Zhou, L., and Zhang, X. Q.: Latitudinal distribution of mixing rate caused by the M-2 internal tide, *J. Phys. Oceanogr.*, 36, 35–42, 2006. 3913
- 20 Timmermann, R. and Hellmer, H. H.: Southern Ocean warming and increased ice shelf basal melting in the 21st and 22nd centuries based on coupled ice-ocean finite-element modelling, *Ocean Dynam.*, in press, 2013. 3936, 3937
- Timmermann, R., Hellmer, H. H., and Beckmann, A.: Simulations of ice-ocean dynamics in the Weddell Sea 2. interannual variability 1985–1993, *J. Geophys. Res.*, 107, 11-1–11-9, doi:10.1029/2000JC000742, 2002. 3915
- 25 Timmermann, R., Danilov, S., Schröter, J., Böning, C., Sidorenko, D., and Rollenhagen, K.: Ocean circulation and sea ice distribution in a finite element global sea ice-ocean model, *Ocean Model.*, 27, 114–129, 2009. 3895, 3900, 3934
- Timmermann, R., Le Brocq, A. M., Deen, T. J., Domack, E. W., Dutrieux, P., Galton-Fenzi, B., Hellmer, H. H., Humbert, A., Jansen, D., Jenkins, A., Lambrecht, A., Makinson, K., Niederjasper, F., Nitsche, F.-O., Nost, O. A., Smedsrud, L. H., and Smith, W.: Antarctic ice sheet topography, cavity geometry, and global bathymetry (RTopo 1.0.5-beta), *Pangaea*, doi:10.1594/PANGAEA.741917, 2010. 3906, 3936
- 30

The Finite Element Sea ice-Ocean Model (FESOM)

Q. Wang et al.

Title Page

Abstract

Introduction

Conclusions

References

Tables

Figures

◀

▶

◀

▶

Back

Close

Full Screen / Esc

Printer-friendly Version

Interactive Discussion



- Timmermann, R., Wang, Q., and Hellmer, H.: Ice-shelf basal melting in a global finite-element sea-ice/ice-shelf/ocean model, *Ann. Glaciol.*, 53, 303–314, 2012. 3904, 3935, 3936, 3937
- Toole, J. M., Schmitt, R. W., Polzin, K. L., and Kunze, E.: Near-boundary mixing above the flanks of a midlatitude seamount, *J. Geophys. Res.-Oceans*, 102, 947–959, 1997. 3912
- 5 Treguier, A. M.: Evaluating eddy mixing coefficients from eddy-resolving ocean models: a case study, *J. Mar. Res.*, 57, 89–108, 1999. 3926
- Treguier, A. M., Held, I. M., and Larichev, V. D.: Parameterization of quasigeostrophic eddies in primitive equation ocean models, *J. Phys. Oceanogr.*, 27, 567–580, 1997. 3924, 3925
- Vage, K., Pickart, R. S., Moore, G. W. K., and Ribergaard, M. H.: Winter mixed layer development in the central iringinger sea: the effect of strong, intermittent wind events, *J. Phys. Oceanogr.*, 38, 541–565, 2008. 3920
- 10 Veronis, G.: The role of models in tracer studies, in: Numerical Models of Ocean Circulation, Ocean Science Committee, National Academy of Sciences, Washington, DC, 133–145, 1975. 3922
- 15 Viebahn, J. and Eden, C.: Towards the impact of eddies on the response of the Southern Ocean to climate change, *Ocean Model.*, 34, 150–165, 2010. 3929
- Visbeck, M., Marshall, J., Haine, T., and Spall, M.: Specification of eddy transfer coefficients in coarse-resolution ocean circulation models, *J. Phys. Oceanogr.*, 27, 381–402, 1997. 3926
- Wang, Q.: The Finite Element Ocean Model and its Aspect of Vertical Discretization, Ph.D. thesis, Bremen University, Bremen, 2007. 3909
- 20 Wang, Q., Danilov, S., and Schröter, J.: Finite Element Ocean circulation Model based on triangular prismatic elements, with application in studying the effect of vertical discretization, *J. Geophys. Res.*, 113, C05015, doi:10.1029/2007JC004482, 2008. 3895, 3896, 3897, 3899, 3900, 3904, 3908, 3919, 3934
- 25 Wang, X., Wang, Q., Sidorenko, D., Danilov, S., Schröter, J., and Jung, T.: Long-term ocean simulations in FESOM: evaluation and application in studying the impact of Greenland Ice Sheet melting, *Ocean Dynam.*, 62, 1471–1486, doi:10.1007/s10236-012-0572-2, 2012. 3901, 3937
- Wekerle, C., Wang, Q., Danilov, S., Jung, T., and Schröter, J.: Freshwater transport through the Canadian Arctic Archipelago in a multi-resolution global model: model assessment and the driving mechanism of interannual variability, *J. Geophys. Res.-Oceans*, submitted, 2013a. 3937
- 30

The Finite Element Sea ice-Ocean Model (FESOM)

Q. Wang et al.

Title Page

Abstract

Introduction

Conclusions

References

Tables

Figures

◀

▶

◀

▶

Back

Close

Full Screen / Esc

Printer-friendly Version

Interactive Discussion



- Wekerle, C., Wang, Q., Danilov, S., Jung, T., Schröter, J., and Myers, P.: The climate relevance of the Canadian Arctic Archipelago: a multi-resolution modeling study, *Geophys. Res. Lett.*, submitted, 2013b. 3902, 3903, 3911, 3937
- White, L., Deleersnijder, E., and Legat, V.: A three-dimensional unstructured mesh finite element shallow-water model, with application to the flows around an island and in a wind-driven, elongated basin, *Ocean Model.*, 22, 26–47, 2008. 3934
- Willebrand, J., Barnier, B., Boning, C., Dieterich, C., Killworth, P. D., Le Provost, C., Jia, Y. L., Molines, J. M., and New, A. L.: Circulation characteristics in three eddy-permitting models of the North Atlantic, *Prog. Oceanogr.*, 48, 123–161, 2001. 3903
- Wunsch, C. and Ferrari, R.: Vertical mixing, energy and the general circulation of the oceans, *Annu. Rev. Fluid Mech.*, 36, 281–314, 2004. 3909, 3912
- Yin, J., Stouffer, R. J., Spelman, M. J., and Griffies, S. M.: Evaluating the uncertainty induced by the virtual salt flux assumption in climate simulations and future projections, *J. Climate*, 23, 80–96, 2010. 3934
- Zhang, J. and Steele, M.: Effect of vertical mixing on the Atlantic Water layer circulation in the Arctic Ocean, *J. Geophys. Res.*, 112, C04S04, doi:10.1029/2006JC003732, 2007. 3913, 3932
- Zhang, R.-H., Busalacchi, A. J., Wang, X., Ballabrera-Poy, J., Murtugudde, R. G., Hackert, E. C., and Chen, D.: Role of ocean biology-induced climate feedback in the modulation of El Niño–Southern Oscillation, *Geophys. Res. Lett.*, 36, L03608, doi:10.1029/2008GL036568, 2009. 3916
- Zhang, Y. L. and Baptista, A. M.: SELFE: a semi-implicit Eulerian–Lagrangian finite-element model for cross-scale ocean circulation, *Ocean Model.*, 21, 71–96, 2008. 3895
- Zhubas, V. and Oh, I. S.: Lateral diffusivity and Lagrangian scales in the Pacific Ocean as derived from drifter data, *J. Geophys. Res.*, 108, 3141, doi:10.1029/2002JC001596, 2003. 3926
- Zienkiewicz, O. C. and Taylor, R. L.: *The Finite Element Method, Vol. 3: Fluid Dynamics*, Butterworth–Heinemann, 5th Edn., Oxford, 2000. 3898
- Zienkiewicz, O. C., Nithiarasu, P., Codina, R., Vazquez, M., and Ortiz, P.: The characteristic-based-split procedure: an efficient and accurate algorithm for fluid problems, *Int. J. Numer. Meth. Fl.*, 31, 359–392, 1999. 3897

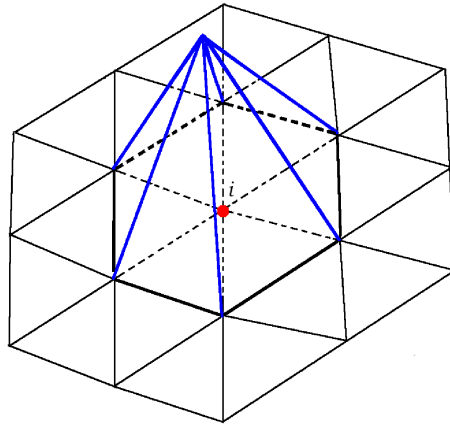


Fig. 1. Schematic of horizontal discretization with the illustration of basis functions used in FESOM. The *stencil* mentioned in the text consists of seven nodes for node i in the example shown in this figure.

GMDD

6, 3893–3976, 2013

The Finite Element Sea ice-Ocean Model (FESOM)

Q. Wang et al.

Title Page

Abstract

Introduction

Conclusions

References

Tables

Figures

◀

▶

◀

▶

Back

Close

Full Screen / Esc

Printer-friendly Version

Interactive Discussion



**The Finite Element
Sea ice-Ocean Model
(FESOM)**

Q. Wang et al.

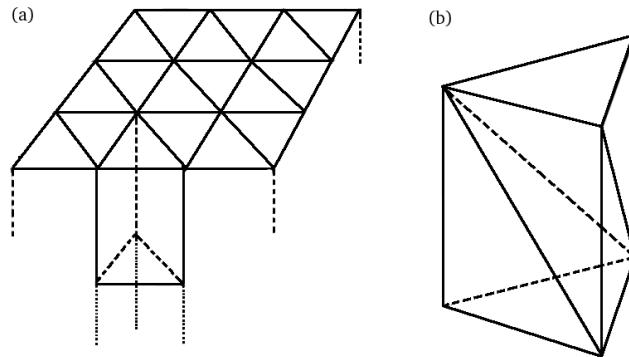


Fig. 2. Schematic of spatial discretization. The column under each surface triangle is cut to prisms **(a)**, which can be divided to tetrahedra **(b)**. Except for layers adjacent to sloping ocean bottom each prism is cut to three tetrahedra.

[Title Page](#)[Abstract](#)[Introduction](#)[Conclusions](#)[References](#)[Tables](#)[Figures](#)[⏪](#)[⏩](#)[◀](#)[▶](#)[Back](#)[Close](#)[Full Screen / Esc](#)[Printer-friendly Version](#)[Interactive Discussion](#)

GMDD

6, 3893–3976, 2013

The Finite Element Sea ice-Ocean Model (FESOM)

Q. Wang et al.

Title Page

Abstract

Introduction

Conclusions

References

Tables

Figures

◀

▶

◀

▶

Back

Close

Full Screen / Esc

Printer-friendly Version

Interactive Discussion

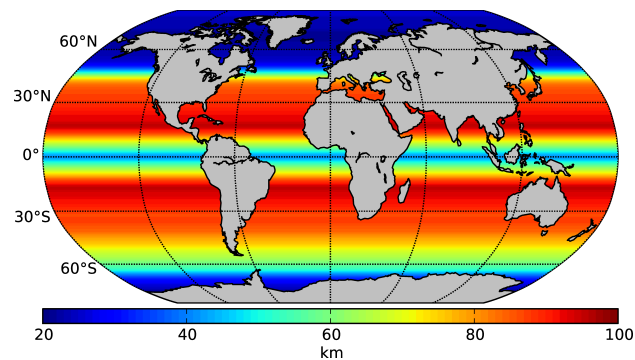


Fig. 3. Horizontal resolution of an example mesh. This mesh is used in all simulations presented in this work.

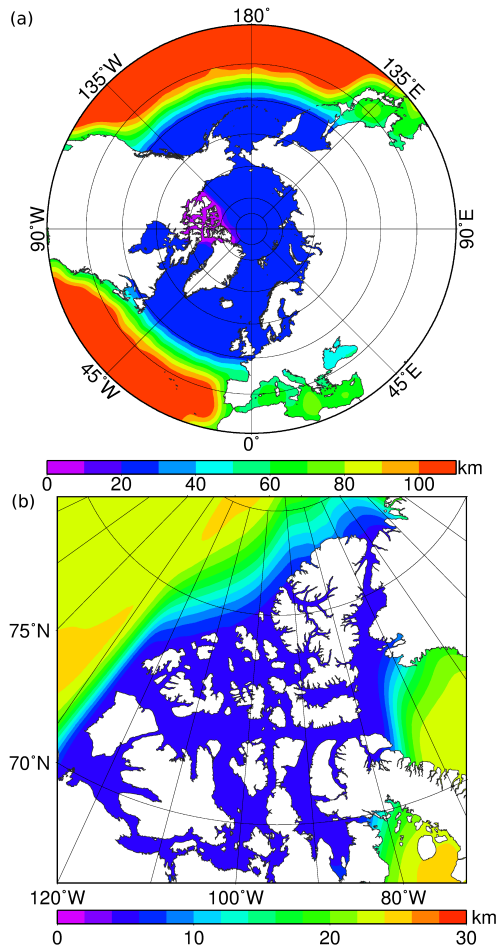


Fig. 4. Horizontal resolution of an example mesh with the CAA region refined: **(a)** view in the stereographic projection and **(b)** zoomed to the CAA region.

The Finite Element Sea ice-Ocean Model (FESOM)

Q. Wang et al.

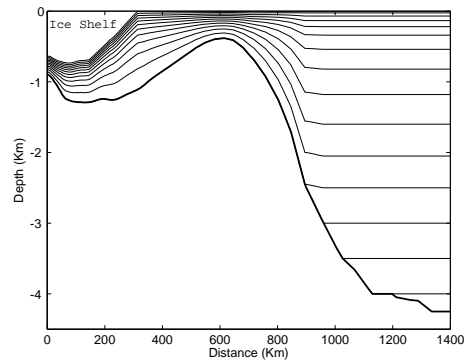


Fig. 5. Schematic of a hybrid vertical grids. The sigma grid is used in adjunction with ice shelf modeling for the Antarctic region, located under the ice shelf and along the continental shelf. Z-level grids are used in other parts of the ocean.

[Title Page](#)[Abstract](#)[Introduction](#)[Conclusions](#)[References](#)[Tables](#)[Figures](#)[◀](#)[▶](#)[◀](#)[▶](#)[Back](#)[Close](#)[Full Screen / Esc](#)[Printer-friendly Version](#)[Interactive Discussion](#)

The Finite Element
Sea ice-Ocean Model
(FESOM)

Q. Wang et al.

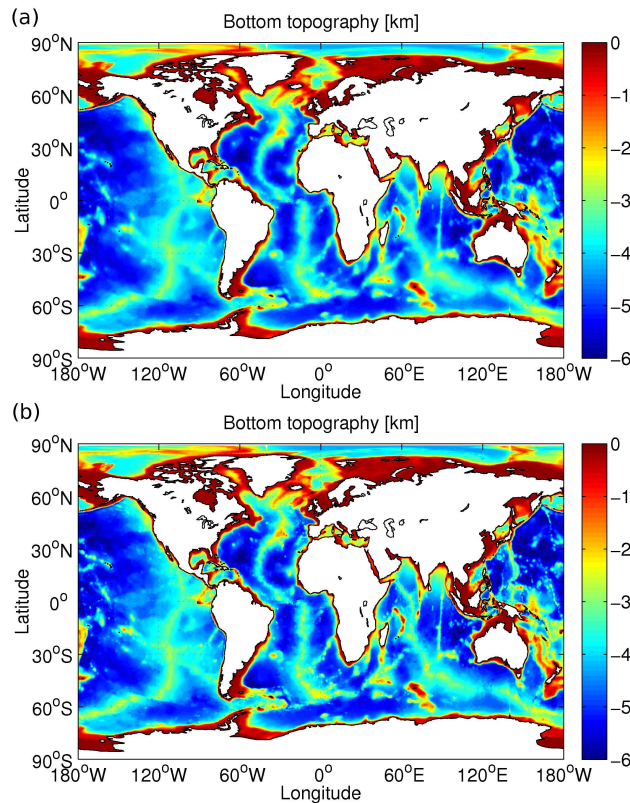


Fig. 6. Bottom topography **(a)** after three iterations of stencil filter and **(b)** after a single iteration.

Title Page

Abstract

Introduction

Conclusions

References

Tables

Figures

◀

▶

◀

▶

Back

Close

Full Screen / Esc

Printer-friendly Version

Interactive Discussion



The Finite Element
Sea ice-Ocean Model
(FESOM)

Q. Wang et al.

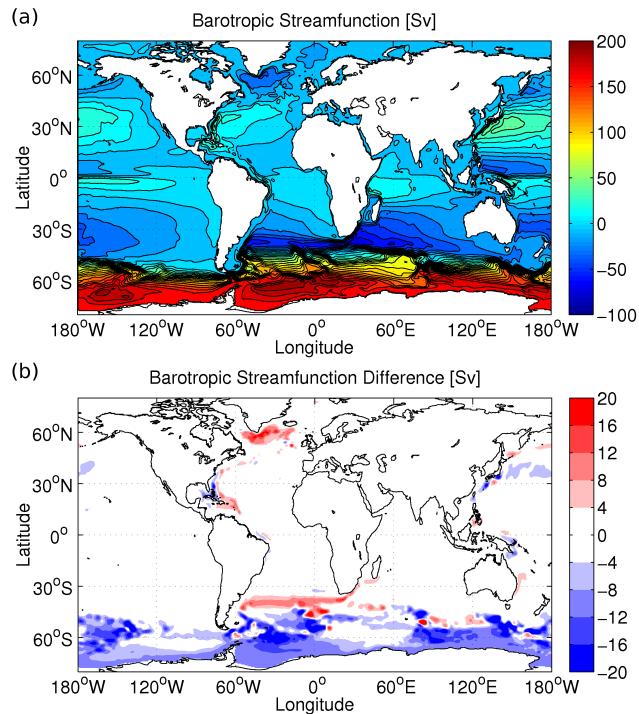


Fig. 7. (a) Barotropic streamfunction (Sv) in a simulation with the topography of Fig. 6a and (b) its difference from a run with the topography of Fig. 6b. Shown are the mean values over the last 10 yr of total 60 yr simulations.

The Finite Element Sea ice-Ocean Model (FESOM)

Q. Wang et al.

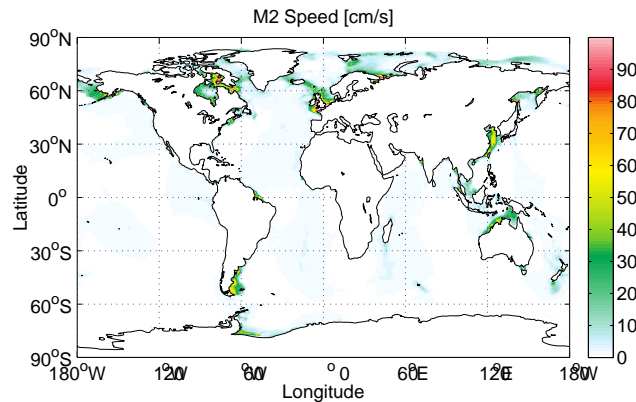


Fig. 8. M2 tidal speed map (cm s^{-1}). High speed is mainly located in shallow shelf regions, including some Arctic and North Atlantic coastal regions.

[Title Page](#)[Abstract](#)[Introduction](#)[Conclusions](#)[References](#)[Tables](#)[Figures](#)[⏪](#)[⏩](#)[◀](#)[▶](#)[Back](#)[Close](#)[Full Screen / Esc](#)[Printer-friendly Version](#)[Interactive Discussion](#)

The Finite Element Sea ice-Ocean Model (FESOM)

Q. Wang et al.

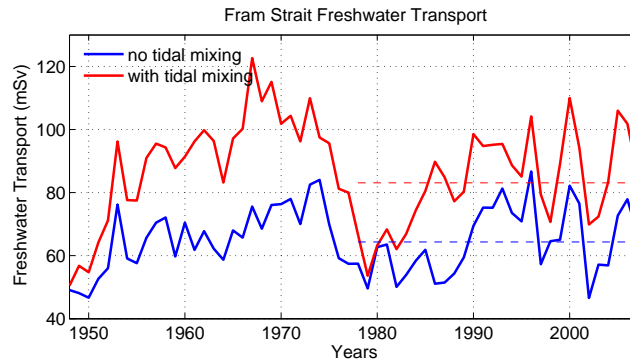


Fig. 9. Time series of Fram Strait freshwater transport (mSv^{-1}). The impact of barotropic tidal mixing is illustrated.

[Title Page](#)[Abstract](#)[Introduction](#)[Conclusions](#)[References](#)[Tables](#)[Figures](#)[⏪](#)[⏩](#)[◀](#)[▶](#)[Back](#)[Close](#)[Full Screen / Esc](#)[Printer-friendly Version](#)[Interactive Discussion](#)

The Finite Element
Sea ice-Ocean Model
(FESOM)

Q. Wang et al.

Title Page

Abstract

Introduction

Conclusions

References

Tables

Figures

◀

▶

◀

▶

Back

Close

Full Screen / Esc

Printer-friendly Version

Interactive Discussion

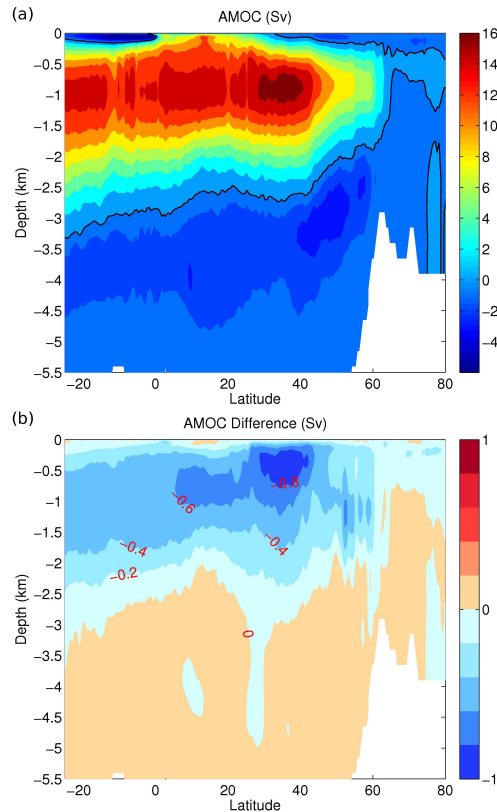


Fig. 10. (a) Atlantic Meridional Overturning Circulation (AMOC) streamfunction (Sv) in a run without parameterized mixing due to barotropic tides and (b) the difference from a run with the tidal mixing. The results are the last 10 yr mean in 60 yr simulations.

The Finite Element Sea ice-Ocean Model (FESOM)

Q. Wang et al.

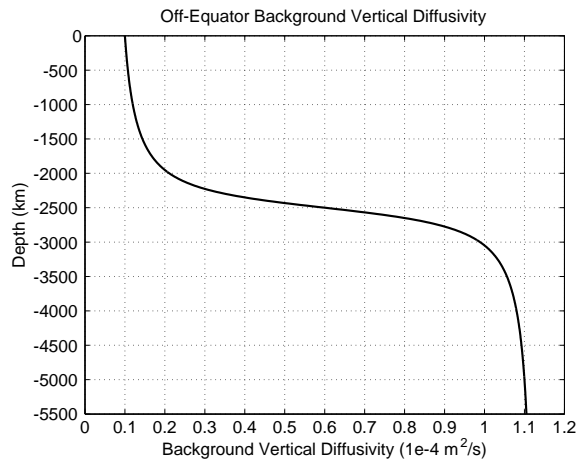


Fig. 11. Background vertical diffusivity poleward of 15° N/S.

Title Page

Abstract	Introduction
Conclusions	References
Tables	Figures

⏪	⏩
◀	▶
Back	Close

Full Screen / Esc

Printer-friendly Version

Interactive Discussion



The Finite Element Sea ice-Ocean Model (FESOM)

Q. Wang et al.

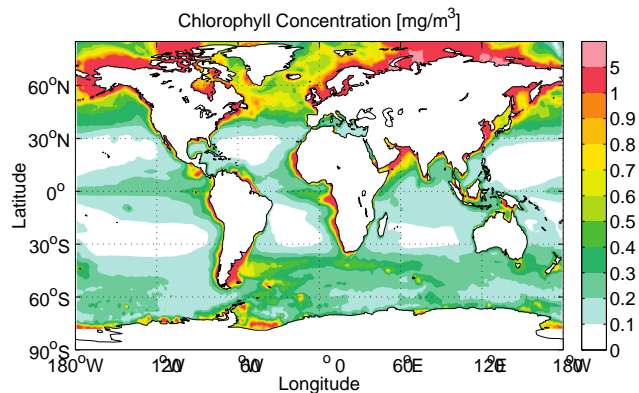


Fig. 12. Annual mean Chlorophyll concentration (mg m^{-3}) climatology. Clear waters are mainly in the subtropical basins and high Chlorophyll concentration is seen in regions with high level of biological activity. The data are from Sweeney et al. (2005).

[Title Page](#)[Abstract](#)[Introduction](#)[Conclusions](#)[References](#)[Tables](#)[Figures](#)[⏪](#)[⏩](#)[◀](#)[▶](#)[Back](#)[Close](#)[Full Screen / Esc](#)[Printer-friendly Version](#)[Interactive Discussion](#)

The Finite Element Sea ice-Ocean Model (FESOM)

Q. Wang et al.

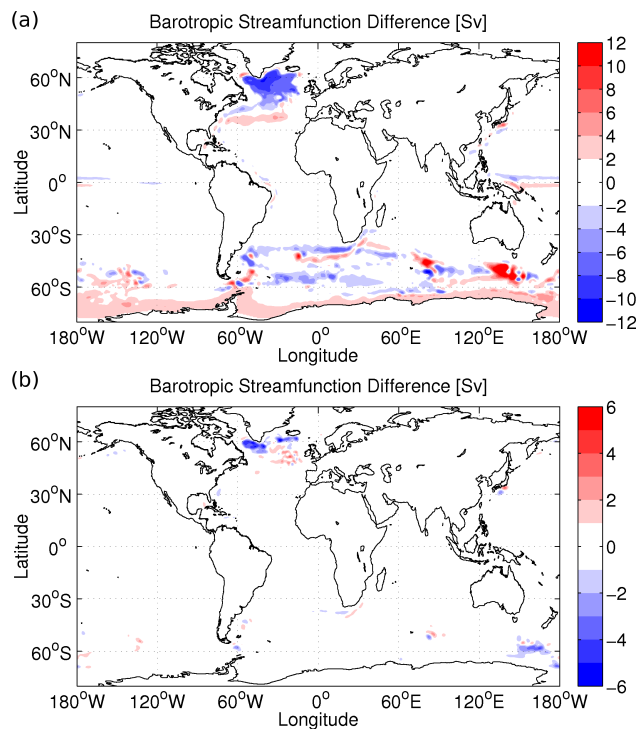


Fig. 13. (a) Barotropic streamfunction difference (Sv) between runs with Laplacian and biharmonic Smagorinsky viscosities (the latter minus former). **(b)** The same as in **(a)** but between a run with biharmonic viscosity scaled with third power of the horizontal resolution and a run with biharmonic Smagorinsky viscosity (the latter minus former). The results are the last 10 yr mean in 60 yr simulations.

[Title Page](#)
[Abstract](#)
[Introduction](#)
[Conclusions](#)
[References](#)
[Tables](#)
[Figures](#)
[Back](#)
[Close](#)
[Full Screen / Esc](#)
[Printer-friendly Version](#)
[Interactive Discussion](#)

The Finite Element Sea ice-Ocean Model (FESOM)

Q. Wang et al.

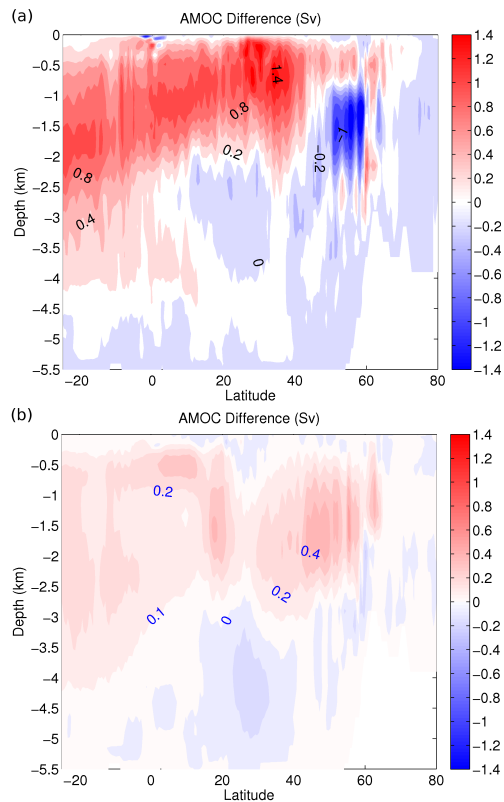


Fig. 14. The same as Fig. 13 but for AMOC (Sv).

Title Page

Abstract

Introduction

Conclusions

References

Tables

Figures

◀

▶

◀

▶

Back

Close

Full Screen / Esc

Printer-friendly Version

Interactive Discussion



The Finite Element Sea ice-Ocean Model (FESOM)

Q. Wang et al.

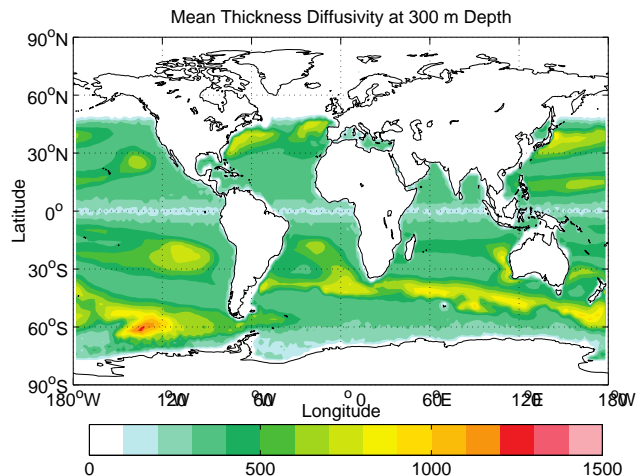


Fig. 15. Ten years mean thickness diffusivity at 300 m depth. The simulation is carried out on the reference mesh shown in Fig. 3.

Title Page

Abstract

Introduction

Conclusions

References

Tables

Figures

◀

▶

◀

▶

Back

Close

Full Screen / Esc

Printer-friendly Version

Interactive Discussion



The Finite Element Sea ice-Ocean Model (FESOM)

Q. Wang et al.

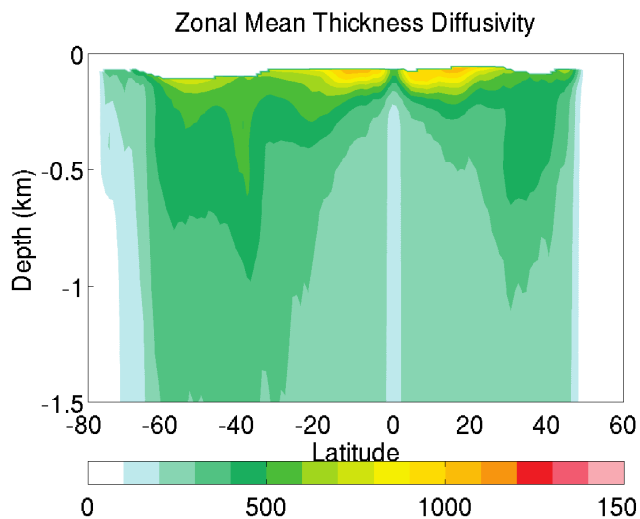


Fig. 16. Zonal mean temporal mean thickness diffusivity. The mean surface boundary layer region is not plotted. The results are the last 10 yr mean in a 60 yr simulation.

[Title Page](#)[Abstract](#)[Introduction](#)[Conclusions](#)[References](#)[Tables](#)[Figures](#)[◀](#)[▶](#)[◀](#)[▶](#)[Back](#)[Close](#)[Full Screen / Esc](#)[Printer-friendly Version](#)[Interactive Discussion](#)

The Finite Element
Sea ice–Ocean Model
(FESOM)

Q. Wang et al.

Title Page

Abstract

Introduction

Conclusions

References

Tables

Figures

◀

▶

◀

▶

Back

Close

Full Screen / Esc

Printer-friendly Version

Interactive Discussion

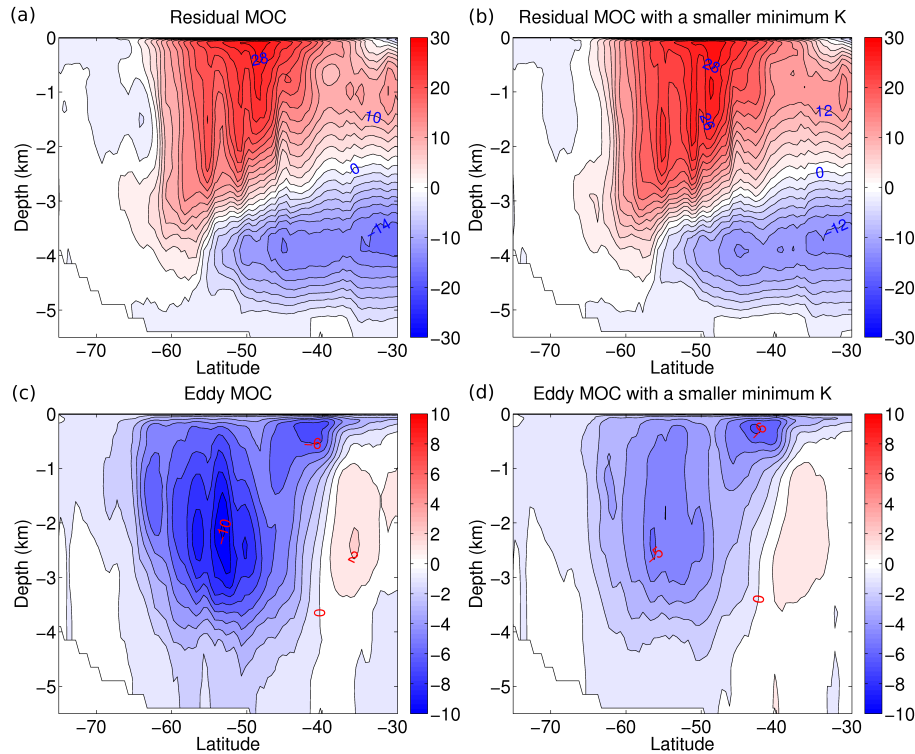


Fig. 17. Residual MOC for **(a)** a reference run and **(b)** a run with a smaller N_{\min} (0.1). **(c)**, **(d)** are the same as **(a)**, **(b)**, respectively, but for the eddy MOC.

The Finite Element Sea ice-Ocean Model (FESOM)

Q. Wang et al.

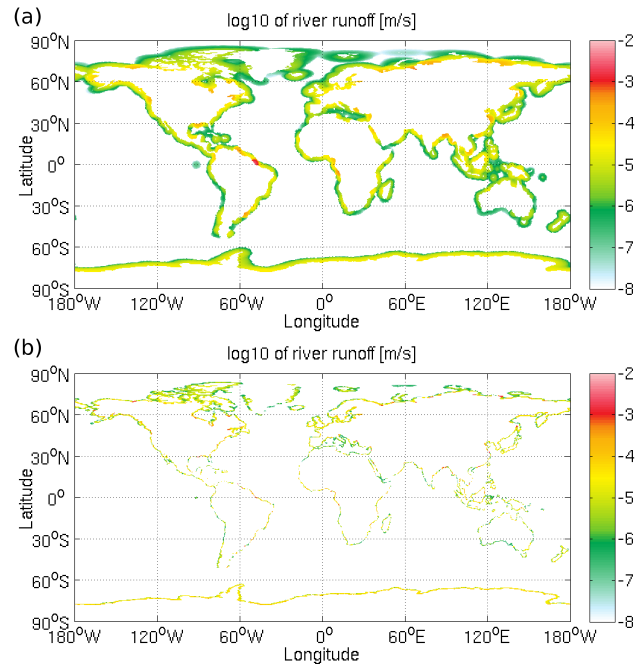


Fig. 18. Annual mean of river runoff climatology (m/s). **(a)** The river runoff is distributed over 400 km distance from river mouths using a linear distribution function. **(b)** The same as **(a)** but over 100 km.

[Title Page](#)
[Abstract](#)
[Introduction](#)
[Conclusions](#)
[References](#)
[Tables](#)
[Figures](#)
[⏪](#)
[⏩](#)
[◀](#)
[▶](#)
[Back](#)
[Close](#)
[Full Screen / Esc](#)
[Printer-friendly Version](#)
[Interactive Discussion](#)

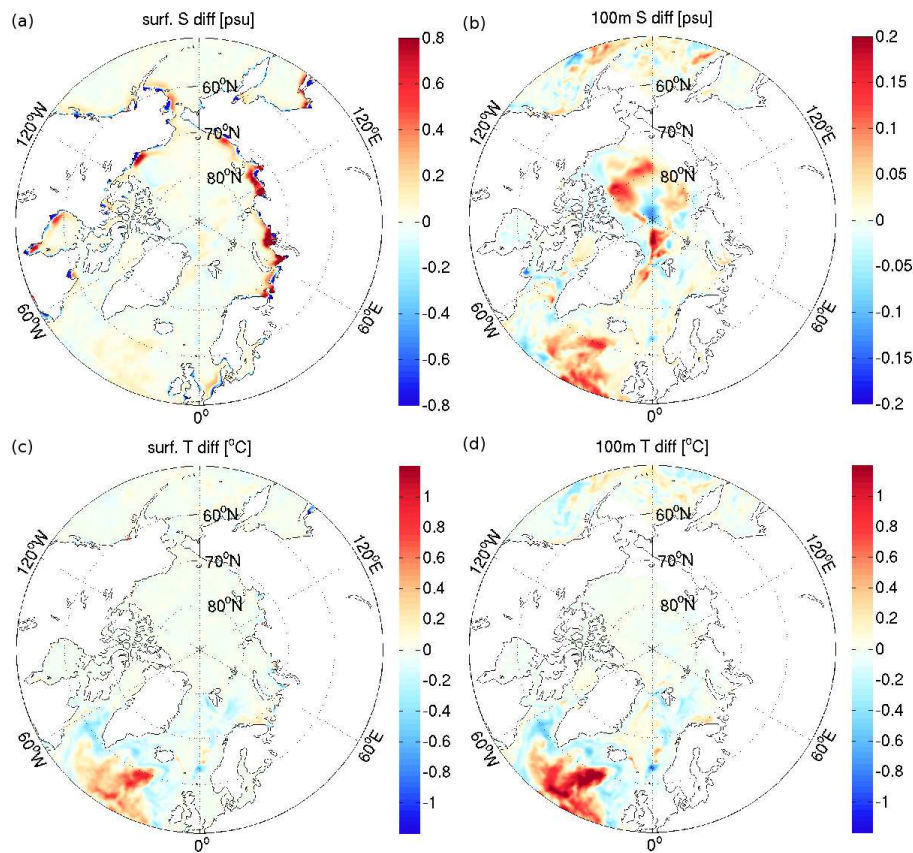



Fig. 19. The salinity difference between runs with river runoff distributed over 400 km and 100 km (the latter minus former) for **(a)** surface and **(b)** 100 m depth. **(c)**, **(d)** The same as **(a)**, **(b)**, respectively, but for temperature. The results are the last 10 yr mean in 60 yr simulations.

The Finite Element Sea ice-Ocean Model (FESOM)

Q. Wang et al.

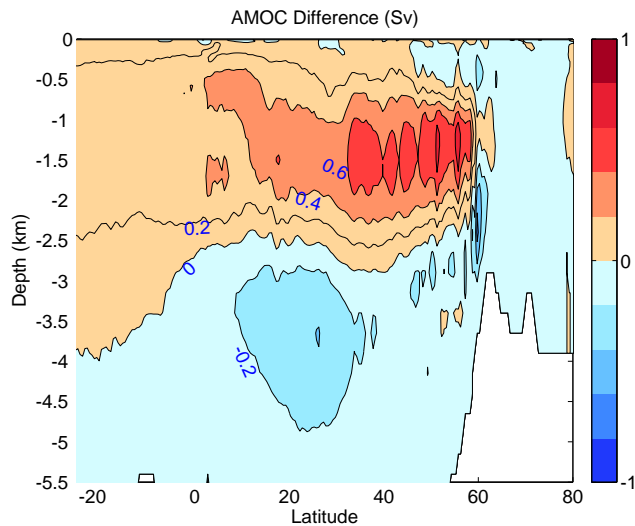


Fig. 20. AMOC difference of a run with river runoff distributed over 400 km distance from a run with a 100 km distribution distance. The results are the last 10 yr mean in a 60 yr simulation.

[Title Page](#)[Abstract](#)[Introduction](#)[Conclusions](#)[References](#)[Tables](#)[Figures](#)[◀](#)[▶](#)[◀](#)[▶](#)[Back](#)[Close](#)[Full Screen / Esc](#)[Printer-friendly Version](#)[Interactive Discussion](#)